Radiosynthesis and in vivo evaluation of a fluorine-18 labeled pyrazine based radioligand for PET imaging of the adenosine A2B receptor

Lindemann, M.; Hinz, S.; Deuther-Conrad, W.; Namasivayam, V.; Dukic-Stefanovic, S.; Teodoro, R.; Toussaint, M.; Kranz, M.; Juhl, C.; Steinbach, J.; Brust, P.; Müller, C. E.; Wenzel, B.;

Originally published:

July 2018

Bioorganic & Medicinal Chemistry 26(2018), 4650-4663

DOI: https://doi.org/10.1016/j.bmc.2018.07.045

Perma-Link to Publication Repository of HZDR:

https://www.hzdr.de/publications/Publ-27386

Radiosynthesis and in vivo evaluation of a fluorine-18 labeled pyrazine based radioligand for PET imaging of the adenosine A_{2B} receptor

Marcel Lindemann[1], Sonja Hinz[2], Winnie Deuther-Conrad[1], Vigneshwaran Namasivayam[2], Sladjana Dukic-Stefanovic[3], Rodrigo Teodoro[1], Magali Toussaint[1], Mathias Kranz[1], Cathleen Juhl[3], Jörg Steinbach[1], Peter Brust[1], Christa E. Müller[2], Barbara Wenzel[1#]

[1] *Helmholtz-Zentrum Dresden-Rossendorf, Institute of Radiopharmaceutical Cancer Research, Department of Neuroradiopharmaceuticals, Leipzig, Germany;*
[2] *Pharma Center Bonn, Pharmaceutical Institute, Pharmaceutical Chemistry I, University of Bonn, Bonn, Germany;*
[3] *ROTOP Pharmaka GmbH, Dresden, Germany*

[#] *corresponding author: b.wenzel@hzdr.de*

Abstract

On the basis of a pyrazine core structure, three new adenosine A_{2B} receptor ligands (**7a** – **c**) were synthesized containing a 2-fluoropyridine moiety suitable for ^{18}F-labeling. Compound **7a** was docked into a homology model of the A_{2B} receptor based on X-ray structures of the related A_{2A} receptor, and its interactions with the adenosine binding site were rationalized. Binding affinity data were determined at the four human adenosine receptor subtypes. Despite a rather low selectivity regarding the A_1 receptor, **7a** was radiolabeled as the most suitable candidate ($K_i(A_{2B})$ = 4.24 nM) in order to perform in vivo studies in mice with the aim to estimate fundamental pharmacokinetic characteristics of the compound class. Organ distribution studies and a single PET study demonstrated brain uptake of **[^{18}F]7a** with a standardized uptake value (SUV) of ≈1 at 5 min post injection followed by a fast wash out. Metabolism studies of **[^{18}F]7a** in mice revealed the formation of a blood-brain barrier penetrable radiometabolite, which could be structurally identified. The results of this study provide an important basis for the design of new derivatives with improved binding properties and metabolic stability in vivo.

Keywords: adenosine A_{2B} receptor, ^{18}F-labeling, pyrazines, metabolism, micellar chromatography

1. Introduction

Adenosine is a purine nucleoside that is released from cells or generated extracellularly following cleavage of adenosine 5'-triphosphate (ATP) by ectonucleotidases.[1] It acts as a signaling molecule and activates four subtypes of G protein-coupled receptors namely, adenosine A_1, A_{2A}, A_{2B}, and A_3 receptors. Each of these receptors exhibits distinct pharmacological properties, cell and tissue distribution, and intracellular signaling.[2, 3]

Activation of the adenosine A_{2B} receptor subtype mediates a stimulation of the adenylate cyclase through coupling to the G_s protein and results in an increase in intracellular cAMP. In addition to G_s coupling, A_{2B} receptors also activate phospholipase C by coupling to G_q proteins leading to an increase in intracellular calcium concentration.[4] Compared to the other adenosine receptors, the A_{2B} receptor is a low-affinity receptor and only activated at adenosine concentrations in the micromolar range.[5, 6] It might therefore not be activated under physiological conditions. However, pathological events (e.g. inflammation, cancer, infection) can lead to elevated adenosine concentrations and increased expression of this receptor subtype.[4] As an example, the contribution of the A_{2B} receptor in cancer progression via mechanisms such as tumor growth, angiogenesis, metastasis and immunomodulation was demonstrated, and its potential as a therapeutic target has recently been reviewed.[4, 7-10]

The tissue distribution and cell expression of A_{2B} receptors have already been investigated by detecting of corresponding mRNA as reviewed elsewhere.[6, 11, 12] Accordingly, a widespread distribution of the A_{2B} receptor gene expression in rats was suggested being highest in colon, cecum, lung, uterus, eye, and bladder.[13, 14] A ubiquitous, low level of mRNA was observed for the brain areas investigated in these studies. In the last decade, A_{2B} receptor expression was also studied in various human tumor cell lines and was found to be high e.g. in prostate, colon carcinoma, neuroendocrine, breast cancer and glioblastoma U87MG cells.[15-19] However, a closer examination of those reports reveals, that there are only very few quantitative data available regarding the actual density of the A_{2B} receptor protein, neither for peripheral organs nor for the brain. To our knowledge, Gessi et al. reported in 2005 on saturation binding experiments using the A_{2B} receptor specific radioligand [^{3}H]MRE 2090-F20.[20] With the determination of B_{max} and K_D values they characterized the expression of the A_{2B} receptor on neutrophils and lymphocytes, cells which are strongly involved in

inflammation. Recently, Hinz et al. reported on A_{2B} receptor expression determined by the radioligand [^{3}H]PSB-603 in native lymphocytes and cancer cell lines.[21]

The main objective of our work is to characterize the expression of the A_{2B} receptor by using positron emission tomography (PET) as a non-invasive molecular imaging technique. The development of a specific radioligand labeled with the PET radionuclide fluorine-18 would support the investigation of this promising target in vitro and in vivo. In particular, it would also be possible to examine the contribution of the A_{2B} receptor in brain tumors and could therefore serve as a basis for a targeting based therapy.

To develop a suitable PET radioligand for this purpose, a lead compound is needed which has i) a high affinity and selectivity for the A_{2B} receptor and ii) the potential to cross the blood-brain barrier (BBB). Several A_{2B} receptor antagonists have been developed in the past and were reviewed elsewhere.[22-24] Most of them are based on the xanthine scaffold such as MRS1754[25], PSB-1115[26], CVT-6883 (GS 6201)[27] and PSB-603[28] (Figure 1). Based on a pyrimidine core, Vidal *et al.* developed LAS38096, a potent non-xanthine based compound which was later structurally optimized leading to the discovery of the pyrazine derivative LAS101057.[29, 30] Recently, the group of Sotelo *et al.* identified with ISAM-140 another novel class of A_{2B} receptor antagonists.[31] In 2016, a carbon-11 labeled triazinobenzimidazole based compound was published,[32] the only A_{2B} receptor targeting PET tracer developed so far (**[^{11}C]2** in Figure 1). With an IC_{50} value of 210 nM obtained with a functional assay by measuring cAMP accumulation, **[^{11}C]2** demonstrates moderate binding toward the A_{2B} receptor. First PET studies in rats showed highest uptake in brown adipose tissue, lungs and testicles. The authors concluded that this compound needs to be further characterized, but may represent an appropriate lead compound for further developments.

In the present study, the pyrazine-based compound class published by Eastwood & Vidal *et al.*[29] was chosen, due to the compounds' potential to penetrate the blood-brain barrier. Accordingly, derivative **1** was selected as a lead compound due to its high affinity and selectivity toward the A_{2B} receptor (Figure 1 & Table 1). Since both fluorine atoms are in positions, which are not activated for a straightforward nucleophilic ^{18}F-labeling, it was decided to substitute the 3-fluoropyridine by a 2-fluoropyridine ring at C5 of the pyrazine ring. Thus, with the new derivative **7a** (Scheme 1) a regioisomer of **1** was developed, in which the fluorine atom is in the *ortho*-position to the pyridine nitrogen. Moreover, the aromatic groups at C6 of the pyrazine ring were modified in order to investigate their

influence on the binding profile. In compound **7b** a more polare pyridine and in **7c** a nonpolar phenyl ring was substituted (Scheme 1).

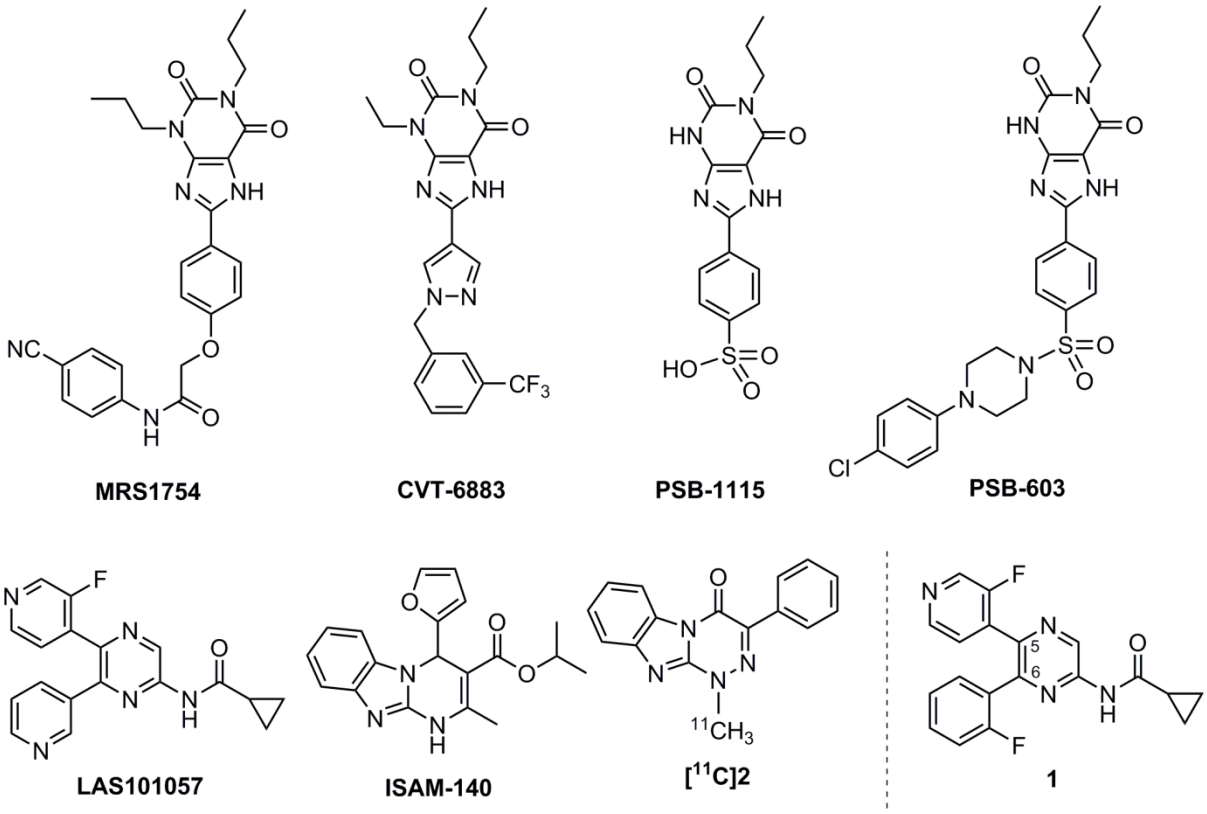

Figure 1. Selected known A_{2B} receptor antagonists, PET radioligand **[^{11}C]2** and lead compound **1**

2. Results and discussion

2.1. Ligand synthesis

Three novel derivatives **7a** - **c** were synthesized which differ regarding their aromatic substituents in position 6 of the pyrazine core. In addition, lead compound **1** was synthesized as a reference[29] to investigate the influence of structural modifications on the in vitro binding affinity toward the four adenosine receptor subtypes.

The syntheses of **1** and the new derivatives **7a** - **c** (Scheme 1) were performed based on the literature.[29, 33] Accordingly, the synthesis route started with the formation of **4**[29] by applying a regioselective iodination of chloropyrazine **3** under mild conditions as described.[29] To obtain **5a**[29] and **5b**, the following metal-catalyzed cross-coupling reaction was performed by two different methods. First, the Stille reaction was applied by using 3-fluoro-4-(tributylstannyl)pyridine and $[Pd(PPh_3)_2Cl_2]$/CuI as described.[29] Second, the Suzuki reaction

was used, because it is beneficial regarding handling and toxicity aspects. Both reactions showed similar yields in the range of 50-60%. Thereafter, the amides **6a**[29] and **6b** were synthesized in pyridine using cyclopropylcarbonyl chloride. In the last step a second Suzuki reaction of **6a** and 2-fluorophenylboronic acid was performed leading to compound **1** in good yields. The amide **6b** served as a precursor molecule for the coupling of different aromatic rings resulting in the new derivatives **7a** - **c** with moderate to high yields.

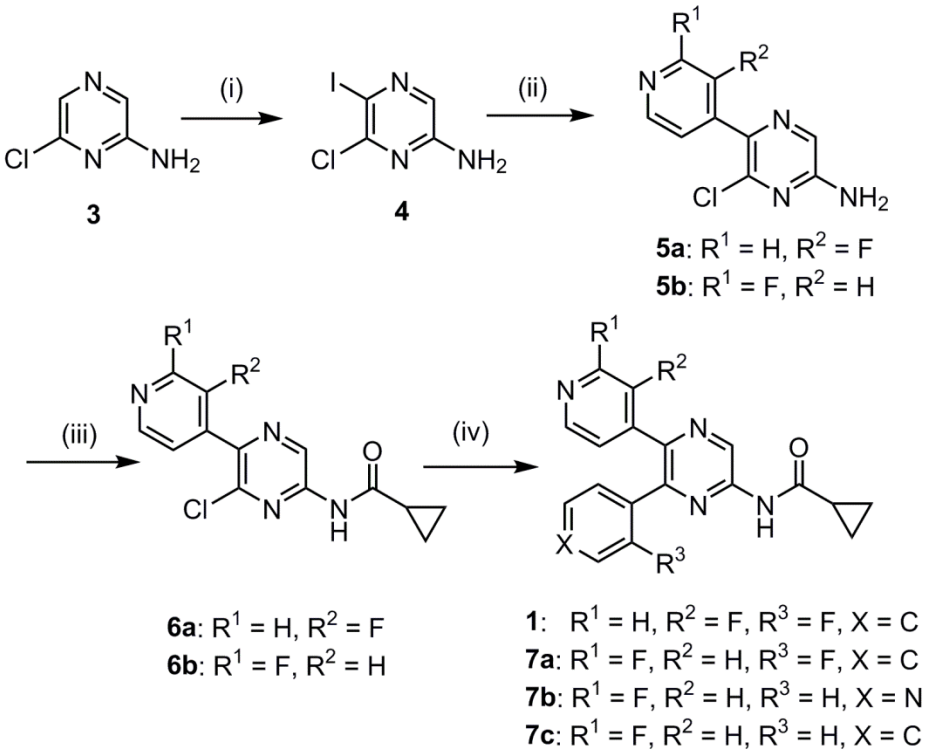

Scheme 1. Synthesis of lead compound **1** and new derivatives **7a** - **c**
Reagents and conditions: (i) *N*-iodosuccinimide, DMSO/H_2O, 88%; (ii) **5a**: 3-fluoro-4-(tributylstannyl)pyridine, [$Pd(PPh_3)_2Cl_2$], CuI, DMF, 150 °C, 61% or 3-fluoro-4-(4,4,5,5-tetramethyl-1,3,2-dioxaborolane-2-yl)pyridine, 2 M Cs_2CO_3, [Pd(dppf)Cl_2], 1,4-dioxane, reflux, 60%; **5b**: 2-fluoropyridine-4-boronic acid, 2 M Cs_2CO_3, [Pd(dppf)Cl_2], 1,4-dioxane, 90 °C, 2 h, 99%; (iii) cyclopropanecarbonyl chloride, pyridine, 80 °C; (iv) 2 M Cs_2CO_3, [Pd(dppf)Cl_2], 1,4-dioxane, **1**: 2-fluorophenylboronic acid, 85 °C, 5.5 h, 64%; **7a**: 2-fluorophenylboronic acid, 90 °C, 7 h, 94%; **7b**: pyridine-4-boronic acid, 90 °C, 2.5 h, 51%; **7c**: phenylboronic acid, 90 °C, 6 h, 61%.

2.2. Determination of in vitro binding affinities

The binding affinities of **1** and **7a** – **c** toward the four adenosine receptor subtypes A_{2B}, A_{2A}, A_1, and A_3 were determined in competition binding assays using membrane preparations of Chinese hamster ovary (CHO) cells expressing the corresponding human receptor subtype and appropriate radioligands (data in Table 1).

In our assay, lead compound **1** showed a high affinity for the A_{2B} receptor (K_i = 1.09 nM) which is similar to the K_i value of 0.6 nM reported by Eastwood *et al.*[29] In general, except for the A_1 receptor, the obtained binding data of **1** are similar to the published data. However, the binding affinity of **1** for the A_1 receptor was 4.6-fold higher than reported (K_i = 28.3 nM versus published 130 nM[29]), which could be due to the different binding assays used. This unexpected drop in selectivity questions the general suitability of **1** as a lead compound.

Compared to **1**, the new derivative **7a** differs in the position of the fluorine substitution at the pyridine ring (3-position in **1** versus 2-position in **7a**). This modification resulted in slight differences in the binding affinities toward the four receptor subtypes. While the affinity of **7a** to the A_{2B} receptor remains high (K_i = 4.24 nM), the selectivities toward A_{2A} and A_1 are decreased resulting in K_i ratios of 1:13 (A_{2B}/A_{2A}) and 1:5 (A_{2B}/A_1).

Eastwood *et al*.[29] already performed a structure-activity relationship study by substituting different aromatic and heteroaromatic ring systems at the 5- and 6-position of the pyrazine core. By using a pyridine substituent in the 6-position a considerable decrease in affinity for A_{2A}, A_1, and A_3 receptors was observed resulting in an increase in A_{2B} selectivity. This prompted us to also modify **7a** by exchanging the 2-fluorophenyl moiety by a pyridine ring to obtain **7b**. However, this modification caused not only the desired decrease in affinities toward the A_{2A}, A_1 and A_3 receptors, but also a considerable loss in affinity for the A_{2B} receptor (K_i = 296 nM). Assuming that the rather polar heteroaromatic ring caused this reduction in binding, which was supported by docking studies (see chapter 2.3.), we synthesized derivative **7c** with a more hydrophobic phenyl ring. With this modification we could indeed obtain a high affinity toward the desired target (K_i = 1.78 nM), however, also the binding affinities to the A_{2A} and A_1 receptors increased considerably resulting in lower selectivities compared to **7a**.

Table 1: K_i values of **1** and **7a** - **c** toward the four adenosine receptor subtypes.

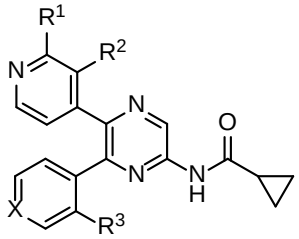

					K_i in nM [a]			
compound	**R^1**	**R^2**	**R^3**	**X**	**A_{2B}**	**A_{2A}**	**A_1**	**A_3**
1	H	F	F	C	1.09 ± 0.20	88.9 ± 25.5	28.3 ± 8.2	937 ± 158
					0.6 ± 0.0 [b]	101 ± 33 [b]	130 ± 44 [b]	8 ± 6% [b, c]
7a	F	H	F	C	4.24 ± 0.04	55.0 ± 6.1	19.0 ± 5.2	796 ± 26
7b	F	H	H	N	296 ± 9.0	1930 ± 400	644 ± 62	>1000
7c	F	H	H	C	1.78 ± 0.25	10.2 ± 1.5	4.29 ± 0.15	680 ± 118

[a] Data are means ± SEM of three independent assays performed in duplicates. Competition binding assays with [^{3}H]PSB-603 (A_{2B}), [^{3}H]MSX-2 (A_{2A}), [^{3}H]CCPA (A_1), and [^{3}H]PSB-11 (A_3) as radioligands and membranes obtained from CHO cells stably expressing the corresponding human adenosine receptor. [b] Data are taken from literature[29] , [c] (%) inhibition at 1 μM of [^{3}H]NECA[29].

2.3. Molecular modelling studies

In order to propose binding modes for the pyrazine derivatives and to rationalize their affinity and selectivity data we selected compound **7a** for performing molecular docking studies using a recently created homology model of the A_{2B} receptor.[34] The putative binding mode of **7a** and the important residues in the binding pocket of the A_{2B} receptor are shown in Figure 2A and 2B, respectively. The model shows that the compound is anchored inside the binding cleft by two key interactions found in all adenosine receptor subtypes. The pyrazine moiety of **7a** likely forms one of the key π-π stacking interactions with F173 and utilizes the hydrophobic surface provided by I276. The second plausible key interaction is the formation of two hydrogen bonds, between the N1 of the pyrazine moiety and the NH of the carboxamido group of **7a** with N254. The pyridine ring attached to the pyrazine (in position 5) is directed towards a pocket formed by the amino acid residues A64, V85, I276 and H280. The nitrogen atom of the pyridine ring possibly introduces a hydrogen bond interaction with H280. The 2-fluorophenyl residue attached in the 6-position of the pyrazine ring is expected

to be in proximity to the highly conserved W247 and is also found to occupy the subpocket formed by V85, L86, T89, M182, W247, V250, and H251. The residues L86, M182, W247 and V250 possibly contribute to hydrophobic interactions with the phenyl ring. The hydrophobic residues in the subpocket favor interactions with the unsubstituted phenyl ring (in **7c**), which showed increased binding affinity in comparison to the more polar pyridine ring (in **7b**). The docking results also indicated that the cyclopropylcarboxamide residue of **7a** further extends to a binding pocket formed by another set of residues comprised of F173, E174, M179, N254, T257, N266, K269 and M272. Among the amino acid residues interacting with **7a** which were discussed above, V250, N266 and K269 are unique for the A_{2B} receptor subtype and could play an important role in determining A_{2B} selectivity (see sequence alignment of the adenosine receptors in Supporting Information, Figure S1).

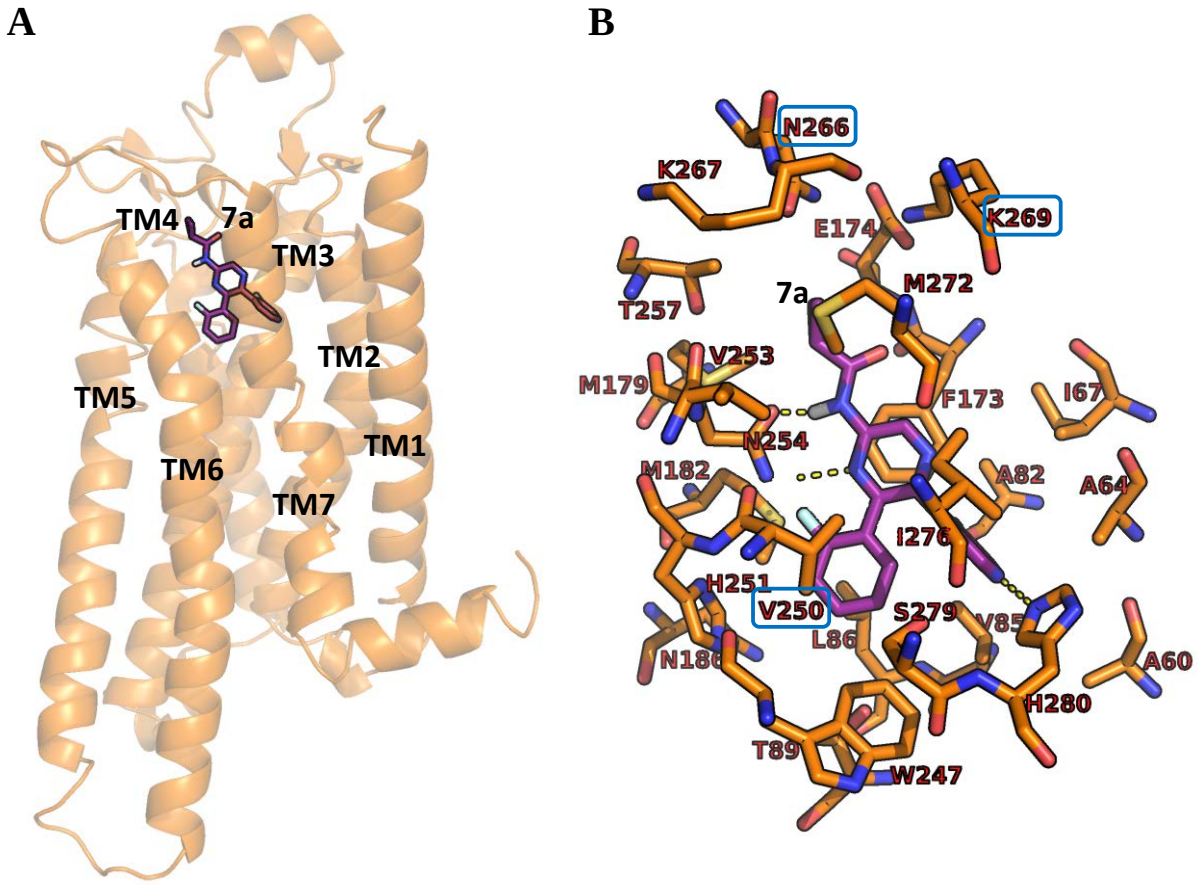

Figure 2. Putative binding mode of **7a** in a homology model of the A_{2B} receptor. **A**) The A_{2B} receptor is represented as cartoon model, and atoms of the docked ligand (**7a**, purple) are depicted as sticks. **B**) The atoms of the docked ligand (**7a**, purple) with important amino acid residues (orange) are depicted as sticks in the binding pocket of the A_{2B} receptor. The amino acids which are unique for the A_{2B} receptor are framed in blue and important interactions are indicated by yellow dotted lines. The oxygen atoms are colored in red, nitrogen atoms in blue, sulfur atoms in yellow and fluorine in cyan.

2.4. Precursor synthesis and radiochemistry

Despite the rather moderate in vitro binding profile of the new derivatives, we decided to radiolabel **7a** as the most promising candidate. The main aim was to examine the general suitability of this substance class by investigating brain uptake and in vivo metabolism.

2.4.1. Synthesis of the precursor

Based on our own experiences,[35] we decided to use a precursor with a nitro leaving group for the intended ^{18}F-labeling. The precursor **13** was generated according to the three step synthesis route depicted in Scheme 2. Starting from compound **4**[29], the amide **8** was synthesized using the same method as for the amides **6a**/**6b**. In the next step, the nitropyridine ring was introduced via a Suzuki reaction of **8** with the dioxaborolane **11**[36] to obtain compound **12**. The borolane **11** was generated in a two-step synthesis, starting with the oxidation of **9** to obtain the known 4-bromo-2-nitropyridine **10** according to a procedure already described.[37] The following Miyaura borylation was performed using [Pd(dppf)Cl_2] as catalyst as reported.[35, 36] In the last step, the 2-fluorophenyl moiety was substituted into compound **12** by using a second Suzuki reaction to obtain the precursor **13**.

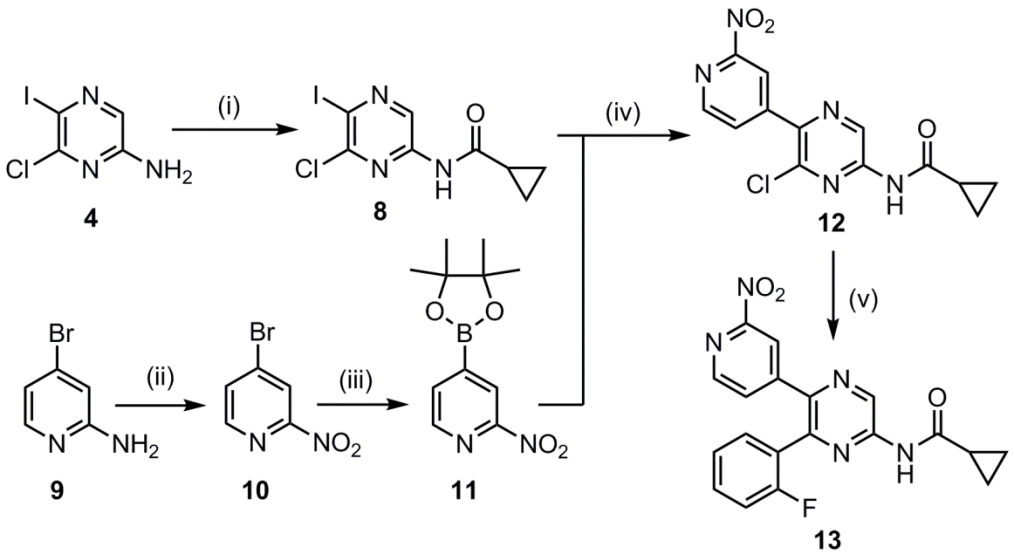

Scheme 2. Synthesis of the precursor **13**

Reagents and conditions: (i) cyclopropanecarbonyl chloride, pyridine, rt, 5.5 h, 90%; (ii) conc. H_2SO_4, 30% H_2O_2, rt, 1 d, 38%; (iii) 4,4,4',4',5,5,5',5'-octamethyl-2,2'-bi-1,3,2-dioxaborolane, KOAc, [Pd(dppf)Cl_2], 1,4-dioxane, reflux, 45 min, 85% (iv) 2 M K_2CO_3, [Pd(dppf)Cl_2], 90 °C, 5 h, 49%; (v) 2-fluorophenylboronic acid, 2 M Cs_2CO_3, [Pd(dppf)Cl_2], 90 °C, 3 h, 61%.

2.4.2. Radiosynthesis and characterization of [^{18}F]7a

Manual synthesis - optimization

For the synthesis of the new radioligand **[^{18}F]7a**, a nucleophilic aromatic substitution reaction of the nitro group of precursor **13** and [^{18}F]fluoride as azeotropically dried kryptofix-carbonate complex was performed. Based on our former experiments with similar aromatic NO_2/[^{18}F]F^- systems,[35, 38] we selected dimethylsulfoxide (DMSO) and *N*,*N*-dimethylformamide (DMF) as the most promising solvents. In a first screening, **[^{18}F]7a** was obtained with comparable results using DMSO and DMF. We went further with DMSO achieving radiochemical yields (RCY) for the labeling process of 58 ± 7% after 20 min at 150 °C (Scheme 3). A considerable decrease of the RCY was observed when reducing the temperature to 120 °C. According to radio-TLC analysis, two radioactive by-products were formed in the reaction mixture accounting for less than 5% of total radioactivity. The precursor remained stable under all conditions tested as proven by HPLC analysis.

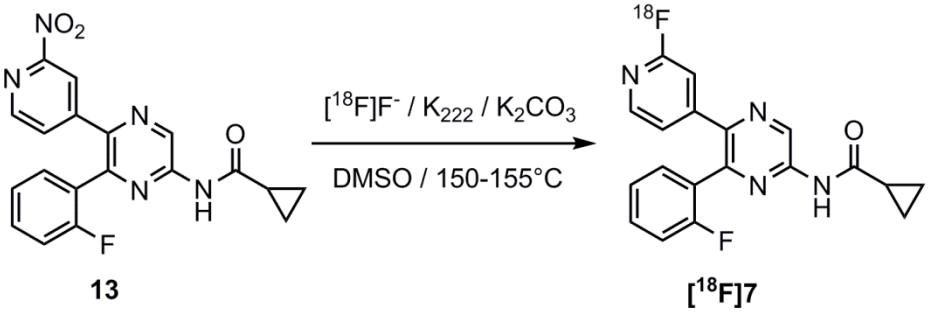

Scheme 3. ^{18}F-labeling of **[^{18}F]7a**

All labeling experiments were performed with a very low amount of precursor (1.0 - 1.2 mg), which was important for the subsequent isolation of the radiotracer by semi-preparative HPLC. The difficulties in the separation arise from the chromatographic similarity of the ^{18}F-labeled compound and its nitro precursor. For the isolation of **[^{18}F]7a** a cyanopropyl-modified column was found to be appropriate using a mixture of acetonitrile (ACN)/water and ammonium acetate as buffer (Figure 3A). By contrast, no separation could be achieved using common strong hydrophobic or polar C18-phases.[39]

*Automated radiosynthesis of **[^{18}F]7a***

On the basis of the manual experiments, the radiosynthesis of **[^{18}F]7a** was translated to an automated procedure using the TRACERlab FX2 N synthesis module (GE Healthcare). The synthesizer setup is described in the experimental part. Briefly, after trapping and elution of [^{18}F]fluoride from an anion exchange cartridge, the labeling reaction of the azeotropically dried [^{18}F]F^-/$K_{2.2.2.}$/K_2CO_3 complex with the precursor **13** was performed in DMSO for 15 min at 150 °C. For isolation of **[^{18}F]7a**, the crude reaction mixture was diluted with aqueous acetonitrile and directly applied to a semi-preparative HPLC system. The radiotracer fraction was collected at a retention time of 30 - 35 min and subjected to a solid phase extraction (SPE) using a C18-cartridge. The obtained radiotracer eluate was transferred out of the hot cell, concentrated and formulated in sterile isotonic saline containing 10% of ethanol. The entire process lasts about 80 - 90 min. Activity balance showed that less than 10% of the radioactivity was lost in the anion exchange cartridge, the reactor and during SPE. Finally, **[^{18}F]7a** could be reproducibly produced with a high radiochemical purity of ≥ 99%, a radiochemical yield of 38.9 ± 1.5% (n = 3) and molar activities between 6 and 8 GBq/µmol (n = 3) at starting activities of 2-3 GBq. Co-injection of the corresponding reference compound **7a** confirmed the identity of **[^{18}F]7a** by analytical radio-HPLC (Figure 3B).

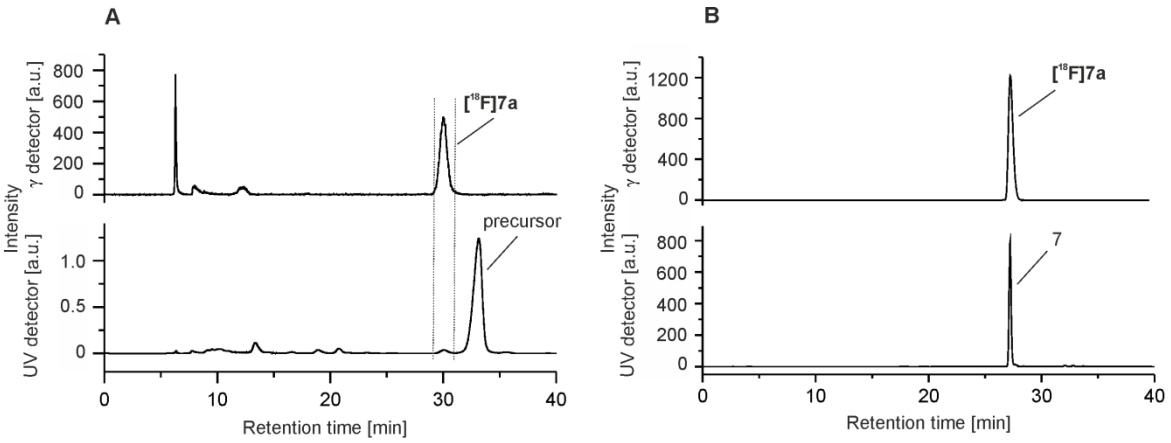

Figure 3. **A**) Semi-preparative radio- and UV-HPLC chromatograms of **[^{18}F]7a** (conditions: Reprosil-Pur CN, 250x20 mm, 40% ACN/20 mM $NH_4OAc_{aq.}$, 8.0 mL/min). **B**) Analytical radio- and UV-HPLC chromatograms of the final product of **[^{18}F]7a** spiked with the non-radioactive reference **7a** (conditions: Reprosil-Pur C18-AQ, 250 x 4.6 mm, gradient with an eluent mixture of ACN/20 mM NH_4OAc aq., 1.0 mL/min).

Stability and logD value of ***[^{18}F]7a***

The stability of the radiotracer was investigated by incubation at 40 °C in *n*-octanol and pig plasma samples. **[^{18}F]7a** proved to be stable in these media, and no defluorination or degradation was observed within 60 min of incubation time.

To estimate the lipophilicity of **[^{18}F]7a**, the logD value was determined by the shake flask method using *n*-octanol and phosphate-buffered saline as partition system. With an obtained logD value of 2.07 ± 0.22 (n = 4) the radiotracer shows a promising physicochemical characteristic with respect to potential PET imaging of the brain.[40-42]

2.5. Specific and selective binding of [^{18}F]7a in vitro

To evaluate if **[^{18}F]7a** binding is (i) specific and (ii) selective to adenosine A_{2B} receptors, mouse brain and heart homogenates were used for binding studies. We observed substantial binding of **[^{18}F]7a** at 4 nM which was significantly blocked by 1 µM **7a** and 1 µM PSB-603 (brain: -80% and -30%; heart: -50% and -20%, respectively). While the blocking observed with **7a** indicates specific binding of **[^{18}F]7a** in rat brain and heart, the comparatively weak efficacy of the selective A_{2B} inhibitor PSB-603 indicates that A_{2B} receptors account for only a fraction of the specific binding sites of the radioligand. Taking into account the nanomolar affinity of **7a** to A_1 and A_{2A} receptors, further binding sites might be related to these receptors which are both highly expressed in brain[43, 44] as well as in cardiomyocytes and cardiac fibroblasts.[45, 46] A supplementary radioligand displacement study (data not shown) using A_1- and A_{2A}-specific tritiated radioligands as well as membrane homogenates of mouse brain and heart supported this assumption as **7a** was able to compete with the respective radioligand for the respective adenosine receptor binding site.

So far and mainly due to the herein detected lack of selectivity, we did not test **[^{18}F]7a** for relevant interaction with additional binding sites not related to adenosine receptors.

2.6. Preliminary in vivo studies of [^{18}F]7a in mouse

2.6.1. Brain uptake and specific binding

Despite the insufficiency of selectivity observed in vitro, we decided to evaluate the ability of **[^{18}F]7a** to penetrate the blood-brain barrier to more thoroughly characterize the suitability of this compound class for the development of PET radiotracers. Therefore, we initially performed organ distribution studies and could show uptake of activity in whole brain

followed by washout (SUV at 5 min p.i.: 0.91 (n=2: 0.81 and 1.00); at 15 min p.i.: 0.60 (n=2: 0.50 and 0.69); and at 30 min p.i.: 0.22 ± 0.04 (n=3)). A preliminary dynamic PET scan performed in one mouse accords with this result (data not shown). However, the distribution of activity at scanning times corresponding to specific binding was rather homogenous (Figure 4A), as also indicated by ex vivo autoradiography performed at 30 min p.i. (Figure 4B). We assume that this result is related to both a low density of A_{2B} receptors under physiological conditions[13] as well as to the low selectivity of the radioligand.

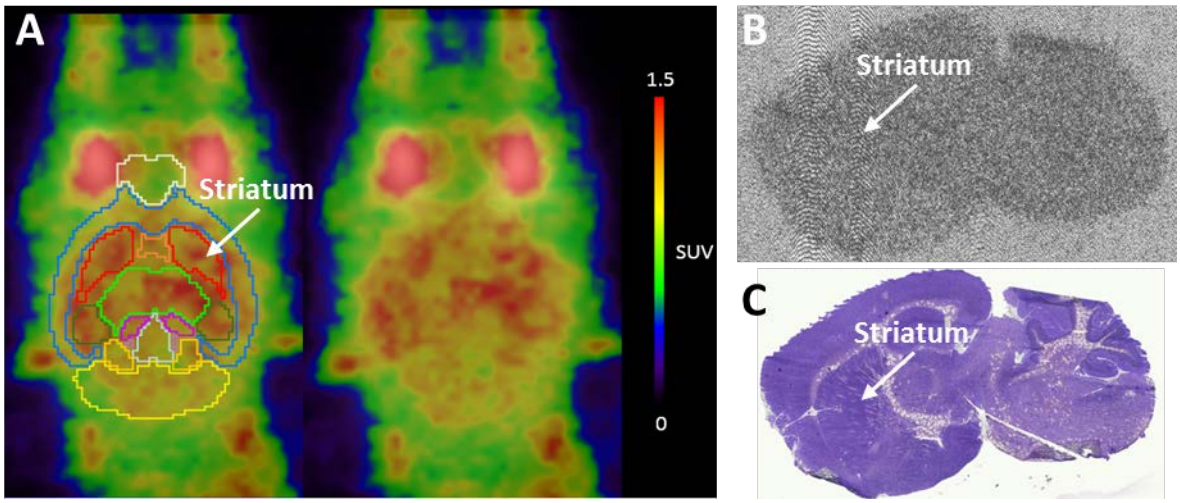

Figure 4. Analysis of the distribution of activity in mouse brain after i.v. injection of **[^{18}F]7a**. **A**) Summed PET image (2 – 15 min p.i. of 3.2 MBq **[^{18}F]7a**) of a mouse brain with atlas superimposed (left). **B**) Autoradiographic image of a sagittal brain slice (10 µm) obtained at 30 min p.i. of 4 MBq **[^{18}F]7a**. **C**) Corresponding Nissl staining.

2.6.2. Metabolism studies

The metabolic stability of **[^{18}F]7a** in vivo was analysed in mice. Blood samples and brains were obtained at 5, 15, and 30 min post i.v. injection of the radiotracer (n = 2 per time point), and plasma and brain samples acquired by centrifugation and homogenization, respectively. Analysis of the samples was performed by using micellar chromatography (MLC) and RP-HPLC. MLC allows to directly inject the samples into the HPLC system without eliminating the tissue matrix due to the ability of micellar aggregates to dissolve the proteins and other components.[47] For RP-HPLC analysis, aliquots of plasma and brain homogenates were treated with a mixture of acetone/water to precipitate the proteins resulting in recoveries of about 90% and 95% of activity for the plasma and brain samples, respectively.

In general, the results obtained with both methods are comparable. A diagram summarizing the chromatographic MLC data is shown in Figure 5A; Figure 5B shows the MLC and RP-HPLC

chromatogram of a plasma sample at 30 min p.i. Accordingly, intact radiotracer accounts for ~35% of total activity in plasma at this time point and four radiometabolites are detected. Only small amounts of [^{18}F]fluoride (**[^{18}F]M1**) are formed, which can be seen in the radio-MLC chromatogram. By contrast, in the corresponding RP-HPLC chromatogram almost no [^{18}F]fluoride could be detected, which is presumably caused by a loss of [^{18}F]fluoride during the extraction process due to a partially non-reversible binding on plasma proteins (lower recovery in plasma samples, see exp. part). The retention of metabolite **[^{18}F]M2** is quite different when comparing the two chromatograms, a phenomenon which is caused by the differences of the separation mechanism of the two chromatographic systems.

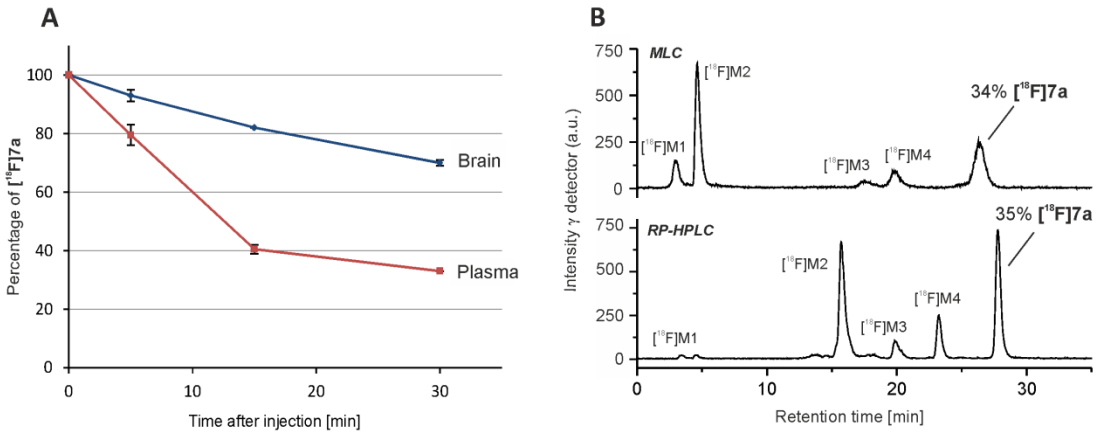

Figure 5. **A**) Percentage of intact radiotracer in dependence of time after injection into mice (n = 2) obtained from radio-MLC chromatographic data. **B**) Exemplary MLC and RP-HPLC radio-chromatograms of a mouse plasma sample at 30 min p.i. of **[^{18}F]7a** (conditions MLC: Reprosil-Pur C18-AQ, 250 x 4.6 mm, gradient with an eluent mixture of THF/100 mM SDS/10 mM $NaHPO_4$aq., 1.0 mL/min; conditions RP-HPLC: Reprosil-Pur C18-AQ, 250 x 4.6 mm, gradient with eluent mixture of ACN/20 mM NH_4OAc aq., 1.0 mL/min).

The most hydrophobic radiometabolite **[^{18}F]M4** is obviously able to penetrate the BBB, because it could be also detected in the brain samples (see B in Figure 6). Thus, 82% of the measured radioactivity in brain at 15 min p.i. and 70% at 30 min p.i. can be assigned to **[^{18}F]7a**.

Eastwood *et al.*[29] already investigated the in vitro metabolism of several pyrazine based derivatives by using rat liver microsomes. They determined a turnover of 75% when incubating lead compound **1** for 30 minutes, which corresponds to our in vivo results of **[^{18}F]7a** in plasma. The authors also described that N- and C-oxidation of the pyridine rings are the major metabolic pathways in vitro and only minor amounts of metabolite are derived from hydrolysis of the amide bond. Since we previously observed in own studies, that the

metabolic degradation in vitro is often faster compared to the in vivo metabolism, the rapid conversion of **[^{18}F]7a** was unexpected. Moreover, the ability of **[^{18}F]M4** to pass the blood-brain barrier prompted us to investigate the molecular structure of this degradation product in order to use this information for the future design of more stable compounds. Therefore, we synthesized the corresponding non-radioactive hydrolysis product **M4** (A in Figure 6). A brain sample obtained at 30 min p.i. of **[^{18}F]7a** in a mouse was spiked with M4 and subjected to MLC measurement. As it can be seen in the corresponding chromatogram B in Figure 6, this amine corresponds to the radiometabolite **[^{18}F]M4**. The calculated logD value of **M4** is 1.71 at physiological pH and could explain the observed permeation of **[^{18}F]M4** across the BBB, since this is within a range which was described to be beneficial for good brain penetration.[40] With a K_i value of 63.0 nM, this radiometabolite still shows affinity for A_{2B} receptors although 15-fold lower than the parent compound **7a** (K_i = 4.24 nM).

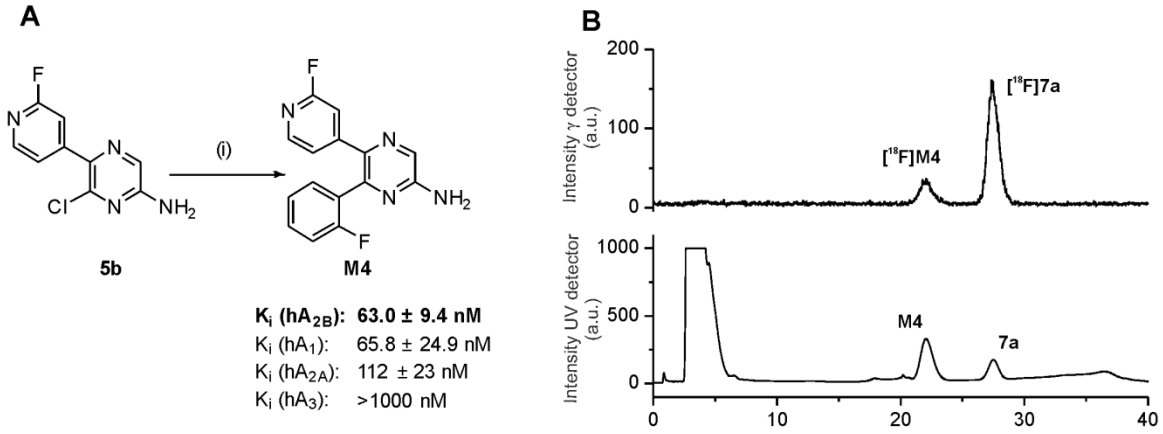

Figure 6. A) Synthesis of the nonradioactive metabolite compound **M4** and its K_i values for the adenosine receptor subtypes (reagents and conditions: (i) (2-fluorophenyl)boronic acid, 2 M Cs_2CO_3, [$PdCl_2$(dppf)], 90 °C, 7 h, 72%). **B**) Analytical radio- and UV-MLC chromatogram of a mouse brain sample at 15 min p.i. of **[^{18}F]7a** spiked with the nonradioactive references **M4** and **7a** (conditions: Reprosil-Pur C18-AQ, 250 x 4.6 mm, gradient with an eluent mixture of THF/100 mM SDS/10 mM $NaHPO_4$ aq., 1.0 mL/min).

3. Summary and conclusion

The objective of this work was to develop an ^{18}F-labeled radiotracer as an imaging probe for characterizing the expression pattern of the adenosine A_{2B} receptor in vitro and in vivo. As our future intention is the use of such radiotracer for investigating brain tumors by non-invasive imaging, we additionally turned our attention to the selection of compounds promising sufficient blood-brain barrier penetration.

Starting with the pyrazine-based derivative **1** [29], which was described to have a high affinity and selectivity for the A_{2B} receptor, we developed the novel derivatives **7a**-**7c** containing a 2-fluoropyridine moiety suitable for nucleophilic ^{18}F-labeling. However, the binding affinity data of the lead compound **1** determined in our radioligand binding assays, did not entirely correspond to the published data[29]; in particular with respect to the affinity toward the A_1 receptor which was considerably higher than reported. This trend was also observed for the new derivatives **7a**-**7c**. Despite the resulting rather low selectivity, we radiolabeled **7a** as most suitable candidate in order to perform initial in vivo studies with the aim to get more information on this substance class regarding brain uptake and metabolic stability. The metabolism studies in mice revealed the formation of a brain penetrable radiometabolite, which could be identified as the corresponding deacylated amine of **[^{18}F]7a** generated by hydrolysis of the amide bond. Preliminary organ distribution studies demonstrated a brain uptake of **[^{18}F]7a** at 5 min p.i. of which we assume to be sufficient for PET imaging.

Our findings show the potential of this substance class regarding brain penetration, physicochemical properties, and pharmacokinetics. However, structural modifications are necessary to improve the selectivity of the compounds toward the A_{2B} receptor subtype as well as the metabolic stability in vivo. Molecular modeling studies based on a recently established homology model of the A_{2B} receptor and published X-ray structures of adenosine A_1 and A_{2A} receptors will support the future design of suitable candidates.

4. Material and methods

4.1. Organic chemistry

4.1.1. General

Analysis of all compounds was performed by MS, HPLC, TLC and NMR spectroscopy. The spectra for the final compounds are given in the supplementary material.

High resolution mass spectra were recorded on an ESI-qTOF Impact II (Bruker Daltonik GmbH) and on an ESI-TOF micrOTOF (Bruker Daltonik GmbH) using ElectroSpray Ionization (ESI). NMR spectra (^{1}H, ^{13}C, ^{13}C-APT, ^{19}F, H,H-COSY, HSQC, HMBC) were recorded on spectrometers from Varian (MERCURY plus 300 MHz, MERCURY plus 400 MHz) and Bruker (AVANCE III HD 400 MHz, DRX-400 400 MHz, Fourier 300 300 MHz). Splitting patterns have been designated as follows: s: singlet, d: doublet, bs: broad singlet, m: multiplet, t: triplet, dd: doublet of doublet, td: triplet of doublet, dt: doublet of triplet.

Analytical thin-layer chromatography was performed on silica gel coated plates (Macherey-Nagel, ALUGRAM SIL G/UV_{254}). The spots were identified by using an UV lamp or by spraying a solution of 0.1% ninhydrin in ethanol/water 1/10 or dipping into a $KMnO_4$-solution (3 g $KMnO_4$, 20 g K_2CO_3, 0.25 ml glacial acid, 300 ml water).

For purification of final products flash column chromatography was used with silica gel ZEOsorb 60/40-63 µm from Apollo Scientific Ltd. and silica gel 40-63 µm from VWR Chemicals.
The chemical purity of the final compounds is ≥ 96% and was controlled by HPLC using a 150 x 3 mm Reprosil-Pur Basic HD – 3 µm column (Dr. Maisch GmbH, Germany). These analytical chromatographic separations were performed on a Dionex Ultimate 3000 system, incorporating a LPG-3400SD pump, an autosampler WPS-3000 TSL, a column compartment TCC-3000SD, a diode array detector DAD3000 (monitoring from 254-720 nm) and a low resolution mass spectrometer MSQ 3000 (Thermo Fisher Scientific Inc., Waltham, USA). A mixture of acetonitrile (ACN) and aqueous 20 mM NH_4OAc was used as eluent in a linear gradient system (0-5 min at 25% ACN, 5-45 min up to 95% ACN, 45-55 min at 95% ACN, 55-57 min up to 25% ACN, 57-65 min at 25%) with a flow of 0.6 mL/min.
Chemical names of compounds were generated by ChemDraw Professional 16.0.

4.1.2. Syntheses

Compound **3** was purchased from Alfa Aesar, Thermo Fisher, Germany. Compound **4** was synthesized according to the literature.[29]

4.1.2.1. 6-Chloro-5-(3-fluoropyridine-4-yl)pyrazine-2-amine ***5a***

Under argon atmosphere, 100 mg of **4** (0.393 mmol, 1.0 eq.) and 130 mg (0.589 mmol, 1.5 eq.) of 3-fluoro-4-(4,4,5,5-tetramethyl-1,3,2-dioxaborolan-2-yl)pyridine (from Fluorochem, UK) were suspended in a mixture of 5 mL 1,4-dioxane and 1.2 mL of a 2 M Cs_2CO_3 solution Afterwards, 28 mg (0.039 mmol, 0.1 eq.) [1,1'-bis(diphenyl-phosphino)ferrocene]dichloropalladium(II) $Pd(dppf)Cl_2$ (from Fluorochem, UK) was added and the reaction mixture was refluxed for 10 h. Further 44 mg (0.196 mmol, 0.5 eq.) of 3-fluoro-4-(4,4,5,5-tetramethyl-1,3,2-dioxaborolan-2-yl)pyridine was added and the mixture was again heated for 2 h. After pouring the mixture into 100 mL water and extraction with ethyl acetate (4 × 25 mL), the combined organic layers were dried over sodium sulfate, filtered and the solvent was evaporated under reduced pressure. The residue was purified by column chromatography (SiO_2, dichloromethane/methanol, 39/1, v/v) to obtain **5a** with a yield of 60% (53 mg, 0.235 mmol).
R_f (SiO_2, dichloromethane/methanol, 19/1, v/v): 0.32; ^{1}H NMR (DMSO-d_6, 400 MHz) δ: 7.31 (s, 2 H); 7.55 (dd, *J* = 6.1 Hz, *J* = 5.2 Hz, 1 H); 7.97 (s, 1 H); 8.53 (d, *J* = 4.8 Hz, 1 H); 8.67 (d, *J* = 1.1 Hz, 1 H) ppm; ^{13}C NMR (DMSO-d_6, 75 Hz) δ: 126.2; 130.3; 131.1; 132.8 (d, *J* = 12.2 Hz); 138.7 (d, *J* = 24.3 Hz); 145.3; 146.3 (d, *J* = 5.1 Hz); 155.9; 156.5 (d, *J* = 256.6 Hz) ppm; ^{19}F NMR (DMSO-d_6, 282 MHz) δ: -128.3 ppm; ESI-MS *m/z* calcd. for $C_9H_7N_4FCl^+$ $[M+H]^+$ 225.0, found 225.1.

4.1.2.2. 6-Chloro-5-(2-fluoropyridine-4-yl)pyrazine-2-amine ***5b***

Under argon atmosphere, 50 mg of **4** (0.196 mmol, 1.0 eq.) and 41 mg of 2-fluoropyridine-4-boronic acid (0.294 mmol, 1.5 eq., from OXCHEM Corporation, USA) was suspended in a

mixture of 3.6 mL 1,4-dioxane and 0.3 mL of a 2 M Cs_2CO_3 solution. Afterwards, 7.2 mg (0.010 mmol, 0.05 eq.) Pd(dppf)Cl_2 was added and the mixture was heated for 2 h at 90 °C. After pouring the mixture into 100 mL water and extraction with ethyl acetate (3 × 25 mL), the combined organic layers were dried over sodium sulfate, filtered and the solvent was evaporated under reduced pressure. The residue was purified by column chromatography (SiO_2, dichloromethane/methanol, 39/1, v/v) to obtain **5b** with a yield of 99% (44 mg, 0.196 mmol).

R_f (SiO_2, dichloromethane/methanol, 39/1, v/v): 0.52; ^{1}H NMR (DMSO-d_6, 300 MHz) δ: 7.36 (s, 2 H), 7.41 (m, 1 H), 7.66 (ddd, *J* = 5.3 Hz, *J* = 2.1 Hz, *J* = 1.4 Hz, 1 H), 7.95 (s, 1 H), 8.27 (d, *J* = 5.3 Hz, 1 H) ppm; ^{13}C NMR (DMSO-d_6, 100 Hz) δ: 108.9 (d, *J* = 39.3 Hz), 121.9 (d, *J* = 3.8 Hz), 131.2, 133.1 (d, *J* = 4.2 Hz), 144.7, 147.8 (d, *J* = 15.6 Hz), 150.5 (d, *J* = 8.8 Hz), 155.6, 163.7 (d, *J* = 234.2 Hz) ppm; ^{19}F NMR (DMSO-d_6, 376 MHz) δ: -68.9 ppm; ESI-MS *m/z* calcd. for $C_9H_7N_4FCl^+$ $[M+H]^+$ 225.03, found 225.03, *m/z* calcd. for $C_9H_6N_4FClNa^+$ $[M+Na]^+$ 247.02, found 247.02.

*4.1.2.3. General procedure for **6a** and **6b**:*

Amine **5a** or **5b** (1 eq.) was dissolved in 0.5 mL dried pyridine and cyclopropanecarbonyl chloride (3.0 eq.) was dropwise added to the solution under ice cooling. After heating for 1 h at 80 °C, the reaction was monitored by TLC until it was completed. Then the solvent was removed under reduced pressure, the residue dissolved in dichloromethane and washed with 5% aqueous sodium hydrogen carbonate solution (1 × 50 mL). The organic layer was separated, dried over sodium sulfate, filtered and concentrated under reduced pressure. The desired product was purified by column chromatography (SiO_2) using a solvent mixture of $CHCl_3$/ethyl acetate, 3/2 (v/v) to get **6a** with a yield of 95% (25 mg, 0.085 mmol). A solvent mixture of dichloromethane/methanol, 49/1 (v/v) was used to get **6b** with a yield of 62% (13 mg, 0.044 mmol).

*4.1.2.3.1. N-(6-Chloro-5-(3-fluoropyridine-4-yl)pyrazine-2-yl)cyclopropanecarboxamide **6a***:

R_f (SiO_2, $CHCl_3$/ethyl acetate, 3/2, v/v): 0.51; ^{1}H NMR ($CDCl_3$, 400 MHz) δ: 1.00-1.06 (m, 2 H), 1.19-1.24 (m, 2 H), 1.65-1.71 (m, 1 H), 7.49 (t, *J* = 5.4 Hz, 1 H), 8.55-8.69 (m, 3 H), 9.57 (s, 1 H) ppm; ^{13}C NMR ($CDCl_3$, 75 MHz) δ: 9.4 (2 C), 15.7, 125.2, 131.8 (d, *J* = 12.4 Hz), 134.2, 139.0 (d, *J* = 24.4 Hz), 140.8, 145.2, 145.8 (d, *J* = 5.2 Hz), 147.1, 156.4 (d, *J* = 260.4 Hz), 172.5 ppm; ^{19}F NMR ($CDCl_3$, 376 MHz) δ: -126.5 ppm; ESI-MS *m/z* calcd. for $C_{13}H_{11}ON_4FCl^+$ $[M+H]^+$ 293.1, found 293.1, calcd. for $C_{13}H_{11}ON_4FClNa^+$ $[M+Na]^+$ 315.0, found 315.0.

*4.1.2.3.2.. N-(6-Chloro-5-(2-fluoropyridine-4-yl)pyrazin-2-yl)cyclopropanecarboxamide **6b***:

R_f (SiO_2, dichloromethane/methanol, 39/1, v/v): 0.53; ^{1}H NMR (DMSO-d_6, 300 MHz) δ: 0.90-0.92 (m, 4 H), 2.01-2.08 (m, 1 H), 7.53 (s, 1 H), 7.74 (d, *J* = 5.2 Hz, 1 H), 8.39 (d, *J* = 5.2 Hz, 1 H), 9.39 (s, 1 H), 11.64 (s, 1 H) ppm; ^{13}C NMR (DMSO-d_6, 100 Hz) δ: 9.1 (2 C), 14.7, 109.9 (d, *J* = 39.5 Hz), 122.5 (d, *J* = 4.0 Hz), 134.2, 142.2 (d, *J* = 3.8 Hz), 143.9, 148.2 (d, *J* = 2.1 Hz), 148.3, 149.5 (d, *J* = 8.5 Hz), 163.5 (d, *J* = 235.1), 173.8 ppm; ^{19}F NMR (DMSO-d_6, 376 MHz) δ: -68.2 ppm; ESI-MS *m/z* calcd. for $C_{13}H_9ON_4FCl^-$ $[M-H]^-$ 291.0, found 291.1.

*4.1.2.4. N-(6-(2-Fluorophenyl)-5-(3-fluoropyridine-4-yl)pyrazine-2-yl)cyclopropanecarboxamide **1**:*

Amide **6a** (91.7 mg, 0.313 mmol, 1.0 eq.) and 2-fluorophenylboronic acid (65.7 mg, 0.470 mmol, 1.5 eq. (from Fluorochem, UK) were added to a solution of 4 mL 1,4-dioxane and 2 mL of a 2 M Cs_2CO_3 solution (4.0 mmol, 12.8 eq.). Under argon atmosphere, 22.7 mg (0.031 mmol, 0.1 eq.) of $Pd(dppf)Cl_2$ was added and the reaction mixture was heated for 5.5 h at 85 °C. Afterwards, the mixture was poured into 100 mL water and filtered over celite. The filtrate was extracted with ethyl acetate (3 × 25 mL) and the combined organic layers were dried over sodium sulfate, filtered and concentrated under reduced pressure. The residue was purified by column chromatography (SiO_2, ethyl acetate/*n*-hexane, 2/3, v/v) to give the desired product **1** with a yield of 64% (71.0 mg, 0.201 mmol).

R_f (SiO_2, ethyl acetate/*n*-hexane, 2/3, v/v): 0.17; Mp: 189.8-191.7 °C; ^{1}H NMR ($CDCl_3$, 300 MHz) δ: 0.91-0.97 (m, 2 H), 1.14-1.19 (m, 2 H), 1.58-1.66 (m, 1 H), 6.94 (t, *J* = 10.0 Hz, 1 H), 7.16 (td, *J* = 7.6 Hz, *J* = 1.1 Hz, 1 H), 7.32-7.44 (m, 3 H); 8.33 (d, *J* = 1.7 Hz, 1 H), 8.43 (d, *J* = 4.9 Hz, 1 H), 8.72 (bs, 1 H), 9.63 (s, 1 H) ppm; ^{13}C NMR ($CDCl_3$, 75 Hz) δ: 9.0 (2 C), 15.6, 115.9 (d, *J* = 21.7 Hz), 124.4 (d, *J* = 3.5 Hz), 125.1 (d, *J* = 14.4 Hz), 125.2, 131.1 (d, *J* = 1.9 Hz), 131.5 (d, *J* = 8.3 Hz), 133.7 (d, *J* = 12.0 Hz), 135.3, 138.6 (d, *J* = 24.8 Hz), 141.9, 145.7 (d, *J* = 5.2 Hz), 147.1, 147.2, 155.9 (d, *J* = 242.8 Hz), 159.3 (d, *J* = 233.5 Hz), 172.6 ppm; ^{19}F NMR ($CDCl_3$, 376 MHz) δ: -115.1, -129.4 ppm; ESI-MS *m/z* calcd. for $C_{19}H_{14}ON_4F_2Na^+$ $[M+Na]^+$ 375.10279, found 375.10250.

*4.1.2.5. General procedure for **7a** – **c**:*

Amide **6b** (1.0 eq.) and 2-fluorophenylboronic acid for **7a** (1.2 eq.), pyridine-4-boronic acid for **7b** (1.2 eq., from Apollo Scientific, UK) or phenylboronic acid for **7c** (1.3 eq., from Merck KGaA, Germany) were added to a solution of 3 mL 1,4-dioxane and 6.0 eq. of a 2 M aqueous Cs_2CO_3 solution. Under argon atmosphere, 0.05 eq. [$Pd(dppf)Cl_2$] was added and the reaction mixture was heated at 90 °C (**7a**: 7 h, **7b**: 2.5 h and **7c**: 6h). Afterwards, the mixture was poured into ~50 mL water and extracted with ethyl acetate (3 × ~25 mL). The combined organic layers were washed with 50 mL brine, dried over anhydrous sodium sulfate, filtered and then concentrated under reduced pressure. The crude product was purified by column chromatography.

*4.1.2.5.1. N-(6-(2-Fluorophenyl)-5-(2-fluoropyridine-4-yl)pyrazine-2-yl)cyclopropanecarboxamide **7a***:

Column chromatography: SiO_2, chloroform/ethyl acetate, 4/1, v/v. Yield: 94% (42.0 mg, 0.119 mmol). R_f (SiO_2, ethyl acetate/*n*-hexane, 2/3, v/v): 0.52; Mp: 156.8-159.8 °C; ^{1}H NMR (DMSO-d_6, 300 MHz) δ: 0.86-0.90 (m, 4 H), 2.04-2.08 (m, 1 H), 7.04 (s, 1 H), 7.15-7.24 (m, 2 H), 7.35 (td, *J* = 7.5 Hz, *J* = 0.9 Hz, 1 H), 7.53 (tdd, *J* = 7.3 Hz, *J* = 5.4 Hz, *J* = 1.8 Hz, 1 H), 7.64 (td, *J* = 7.5 Hz, *J* = 1.8 Hz, 1 H), 8.15 (d, *J* = 5.2 Hz, 1 H), 9.45 (s, 1 H), 11.48 (s, 1 H) ppm; ^{13}C NMR (DMSO-d_6, 100 Hz) δ: 8.8 (2 C), 14.6, 108.9 (d, *J* = 39.4 Hz), 116.2 (d, *J* = 21.1 Hz), 121.7 (d, *J* = 3.7 Hz), 125.4 (d, *J* = 3.0 Hz), 125.4 (d, *J* = 15.1 Hz), 132.4 (d, *J* = 2.3 Hz), 132.4 (d, *J* = 11.3 Hz), 135.2, 143.9 (d, *J* = 3.8 Hz), 145.9, 148.0 (d, *J* = 15.5 Hz), 148.4, 151.7 (d, *J* = 9.2 Hz), 159.0 (d, *J* = 247.0 Hz), 163.5 (d, *J* = 234.8 Hz), 173.8 ppm; ^{19}F NMR (DMSO-d_6, 282 MHz)

δ: -115.7, -68.5 ppm; ESI-MS *m/z* calcd. for $C_{19}H_{15}ON_4F_2^+$ $[M+H]^+$ 353.12084, found 353,12091, *m/z* calcd. for $C_{19}H_{14}ON_4F_2Na^+$ $[M+Na]^+$ 375.10279, found 375.10274.

*4.1.2.5.2. N-(5-(2-Fluoropyridine-4-yl)-6-(pyridine-4-yl)pyrazine-2-yl)cyclopropane-carboxamide **7b**:*

Column chromatography: SiO_2, chloroform/methanol, 12/1, v/v. Yield: 51% (39 mg, 0.116 mmol). R_f (SiO_2, chloroform/methanol, 12/1, v/v): 0.44; Mp: 239.7-240.5 °C (decomposition); ^{1}H NMR (DMSO-d_6, 300 MHz) δ: 0.90-0.92 (m, 4 H), 2.06-2.13 (m, 1 H), 7.16 (s, 1 H), 7.25 (d, *J* = 5.1 Hz, 1 H), 7.44 (d, *J* = 4.4 Hz, 2 H), 8.19 (d, *J* = 5.2 Hz, 1 H), 8.63 (d, *J* = 4.2 Hz, 2 H), 9.46 (s, 1 H), 11.50 (s, 1 H) ppm; ^{13}C NMR (DMSO-d_6, 100 Hz) δ: 8.9 (2C), 14.6, 110.1 (d, *J* = 39.1 Hz), 122.8 (d, *J* = 3.7 Hz), 124.5 (2C), 135.3, 143.2 (d, *J* = 3.5 Hz), 145.0, 148.1 (d, *J* = 16.2 Hz), 148.2, 148.6, 150.3 (2C), 151.5 (d, *J* = 8.3 Hz), 163.5 (d, *J* = 235.2 Hz), 173.8 ppm; ^{19}F NMR (DMSO-d_6, 376 MHz) δ: -68.2 ppm; ESI-MS *m/z* calcd. for $C_{18}H_{15}ON_5F^+$ $[M+H]^+$ 336.12551, found 336.12527.

*4.1.2.5.3. N-(5-(2-Fluoropyridine-4-yl)-6-phenylpyrazine-2-yl)cyclopropanecarboxamide **7c**:*

Column chromatography: SiO_2, ethyl acetate/*n*-hexane, 1/3, v/v. Yield: 61% (35 mg, 0.105 mmol). R_f (SiO_2, ethyl acetate/*n*-hexane, 1/3, v/v): 0.29; Mp: 160.9-162.2 °C; ^{1}H NMR (DMSO-d_6, 300 MHz) δ: 0.91-0.97 (m, 2 H), 1.14-1.19 (m, 2 H), 1.58-1.63 (m, 1 H), 7.02 (s, 1 H), 7.13 (dt, *J* = 5.2 Hz, *J* = 1.6 Hz, 1 H), 7.35-7.41 (m, 5 H), 8.09 (d, *J* = 5.2 Hz, 1 H), 8.50 (s, 1 H), 9.54 (s, 1 H) ppm; ^{13}C NMR (DMSO-d_6, 75 Hz) δ: 9.0 (2 C), 15.7, 109.9 (d, *J* = 38.8 Hz), 121.8 (d, *J* = 4.1 Hz), 128.7 (2 C), 129.35 (2 C), 129.59, 134.4, 136.9, 143.5 (d, *J* = 3.6 Hz), 146.8, 147.4 (d, *J* = 15.0 Hz), 150.6, 151.5 (d, *J* = 3.6 Hz), 163.9 (d, *J* = 238.5 Hz), 172.5 ppm; ^{19}F NMR (DMSO-d_6, 282 MHz) δ: -67.5 ppm; ESI-MS *m/z* calcd. for $C_{19}H_{16}ON_4F^+$ $[M+H]^+$ 335.13027, found 335.13023.

*4.1.2.6. N-(6-Chloro-5-iodopyrazine-2-yl)cyclopropanecarboxamide **8**:*

Amine **4** (200 mg, 0.786 mmol, 1.0 eq.) was dissolved in dried pyridine and cyclopropanecarbonyl chloride (85 µL, 98 mg, 0.943 mmol, 1.2 eq.) was dropwise added to the solution under ice cooling. After stirring for 2.5 h at room temperature, the reaction was monitored by TLC and further cyclopropanecarbonyl chloride (58 µL, 66 mg, 0.631 mmol, 0.78 eq.) was added until the reaction was completed. Then the solvent was removed under reduced pressure, the residue suspended in 50 mL water and extracted with ethyl acetate (3 × 50 mL). The organic layers were separated, dried over sodium sulfate, filtered and concentrated under reduced pressure. The desired product **8** was purified by column chromatography (SiO_2) using a solvent mixture of dichloromethane/methanol, 39/1, v/v to get **8** with a yield of 90% (280 mg, 0.711 mmol).

R_f (SiO_2, dichloromethane/methanol, 99/1, v/v): 0.79; Mp: 186.7-187.8 °C; ^{1}H NMR (DMSO-d_6, 400 MHz) δ: 0.86-0.90 (m, 4 H), 1.94-2.02 (m, 1 H), 9.08 (s, 1 H), 11.45 (s, 1 H) ppm; ^{13}C NMR (DMSO-d_6, 100 Hz) δ: 9.0 (2 C), 14.7, 106.4, 135.2, 147.6, 150.5, 173.5 ppm; ESI-MS *m/z* calcd. for $C_8H_8N_3PClI^+$ $[M+H]^+$ 323.940, found 323.939, *m/z* calcd. for $C_8H_7N_3OClINa^+$ $[M+Na]^+$ 345.921, found 345.921, *m/z* calcd. for $C_8H_6N_3OClI^-$ $[M-H]^-$ 321.925, found 321.925.

*4.1.2.7. 4-Bromo-2-nitropyridine **10**:*

A mixture of 2.5 mL of a 30% hydrogen peroxide solution and 5.0 mL of 96% sulfuric acid was added to a solution of 1.5 mL of 96% sulfuric acid and 0.52 g (3.006 mmol) **9** (2-amino-4-bromopyridine from Fluorochem, UK). After one day stirring at room temperature the solution was diluted with 100 mL water and adjusted to a pH value of 12 using 6 M aqueous NaOH. The water phase was extracted with ethyl acetate (3 × 50 mL) and the combined organic layers were washed with brine, dried over sodium sulfate, filtered and the solvent was evaporated under reduced pressure. The crude product was purified by column chromatography (SiO_2, ethyl acetate/*n*-hexane, 2/1, v/v), to get **10** with a yield of 38% (0.23 g, 1.143 mmol).

R_f (SiO_2, ethyl acetate/*n*-hexane, 1/3, v/v): 0.43; Mp: 49.5-50.6 °C; ^{1}H NMR (DMSO-d_6, 400 MHz) δ: 8.20 (dd, *J* = 5.1 Hz, *J* = 1.6 Hz, 1 H), 8.56 (d, *J* = 1.5 Hz, 1 H), 8.58 (d, *J* = 5.1 Hz, 1 H) ppm; ^{13}C NMR (DMSO-d_6, 100 Hz) δ: 122.0, 133.3, 135.7, 150.2, 157.3 ppm; ESI-MS *m/z* calcd. for $C_5H_3O_2N_2BrNa^+$ $[M+Na]^+$ 224.9, found 224.9.

*4.1.2.8. 2-Nitro-4-(4,4,5,5-tetramethyl-1,3,2-dioxaborolane-2-yl)pyridine **11**[36]:*

Under argon atmosphere, 0.20 g (0.985 mmol, 1.0 eq.) of **10**, 0.25 g (0.985 mmol, 1.0 eq.) 4,4,4',4',5,5,5',5'-octamethyl-2,2'-bi-1,3,2-dioxaborolane (from Frontier Scientific, USA) and 0.48 g (4.925 mmol, 5.0 eq.) potassium acetate are mixed in 12 mL 1,4-dioxane. Then 0.03 g (0.039 mmol, 0.04 eq.) Pd(dppf)Cl_2 was added and the reaction mixture was refluxed for 45 min. After cooling to room temperature, the solution was filtered over celite and washed with 50 mL 1,4-dioxane. The solvent was evaporated under reduced pressure and the crude product was purified by column chromatography (SiO_2, ethyl acetate/*n*-hexane, 1/1, v/v), to get **11** with a yield of 85% (0.21 g, 0.840 mmol).

R_f (SiO_2, ethyl acetate/*n*-hexane, 1/1, v/v): 0.05; Mp: 111.0-117.4 °C; ^{1}H NMR ($CDCl_3$, 400 MHz) δ: 1.37 (s, 12 H), 7.98 (dd, *J* = 4.5 Hz, *J* = 0.7 Hz, 1 H), 8.56 (s, 1 H), 8.65 (dd, *J* = 4.5 Hz, *J* = 0.8 Hz, 1 H) ppm; ^{13}C NMR ($CDCl_3$, 100 Hz) δ: 24.8 (4 C), 85.3 (2 C), 122.7, 134.2, 148.4, 156.6 ppm; ESI-MS *m/z* calcd. for $C_{11}H_{15}O_4N_2BNa^+$ $[M+Na]^+$ 273.1, found 273.1, *m/z* calcd. for $C_{22}H_{30}O_8N_4B_2Na^+$ $[2M+Na]^+$ 523.2, found 523.2.

*4.1.2.9. N-(6-Chloro-5-(2-nitropyridine-4-yl)pyrazine-2-yl)cyclopropanecarboxamide **12**:*

Under argon atmosphere, 200 mg (0.618 mmol, 1.0 eq.) of **8** and 170 mg (0.680 mmol, 1.1 eq.) of **11** are dissolved in a mixture of 5 mL 1,4-dioxane and 1.24 mL (2.472 mmol, 4.0 eq.) 2 M aqueous potassium carbonate solution. Then 9.0 mg (0.012 mmol, 0.02 eq.) Pd(dppf)Cl_2 was added and the reaction mixture was heated for 5 h at 90 °C. After cooling to room temperature, the reaction mixture was quenched with 100 mL water and extracted with ethyl acetate (3 × 25 mL). The combined organic layers were dried over sodium sulfate, filtered and the solvent was evaporated under reduced pressure. The crude product was purified by column chromatography (SiO_2, ethyl acetate/*n*-hexane, 2/3, v/v) to give **12** with a yield of 49% (97 mg, 0.303 mmol).

R_f (SiO_2, ethyl acetate/*n*-hexane, 2/3, v/v):0.50 °C; Mp: 172.5-175.5 °C; ^{1}H NMR (DMSO-d_6, 400 MHz) δ: 0.89-0.91 (m, 4 H), 1.99-2.05 (m, 1 H), 8.28 (dd, *J* = 4.9 Hz, *J* = 1.4 Hz, 1 H), 8.63

(d, *J* = 0.9 Hz, 1 H), 8.80 (d, *J* = 5.0 Hz, 1 H), 9.37 (s, 1 H), 11.64 (s, 1 H) ppm; ^{13}C NMR (DMSO-d_6, 100 Hz) δ: 9.1 (2 C), 14.7, 118.2, 129.7, 134.3, 141.2, 144.1, 147.9, 148.4, 149.6, 157.1, 173.8 ppm; ESI-MS *m/z* calcd. for $C_{13}H_{11}N_5O_3Cl^+$ $[M+H]^+$ 320.054, found 320.054, *m/z* calcd. for $C_{13}H_{10}N_5O_3ClNa^+$ $[M+Na]^+$ 342.036, found 342.036, *m/z* calcd. for $C_{26}H_{20}N_{10}O_6Cl_2Na^+$ $[2M+Na]^+$ 661.084, found 661.084, *m/z* calcd. for $C_{13}H_9N_5O_3Cl^-$ $[M-H]^-$ 318.040, found 318.040.

*4.1.2.10. N-(6-(2-Fluorophenyl)-5-(2-nitropyridine-4-yl)pyrazine-2-yl)cyclo-propanecarboxamide **13**:*

Amide **12** (70 mg, 0.219 mmol, 1.0 eq.) and 2-fluorophenylboronic acid (40 mg, 0.285 mmol, 1.3 eq.) were added to a mixture of 5 mL 1,4-dioxane and 660 µl of a 2 M Cs_2CO_3 solution (1.314 mmol, 6.0 eq.). Under argon atmosphere, 8.0 mg (0.011 mmol, 0.05 eq.) Pd(dppf)Cl_2 was added and the reaction mixture was heated 3 h at 90 °C. After cooling to room temperature, the mixture was poured into 50 mL water and extracted with ethyl acetate (3 × 30 mL). The combined organic layers were dried over anhydrous sodium sulfate, filtered and concentrated under reduced pressure. The crude product was purified by column chromatography (SiO_2, ethyl acetate/*n*-hexane, 2/3, v/v) to give the desired product **13** with a yield of 61% (64 mg, 0.158 mmol).

R_f (SiO_2, ethyl acetate/*n*-hexane, 2/3, v/v): 0.35; Mp: 134.7-137.0 °C; ^{1}H NMR (DMSO-d_6, 400 MHz) δ: 0.85-096 (m, 4 H), 2.04-2.14 (m, 1 H), 7.21 (t, *J* = 8.0 Hz, 1 H), 7.40 (t, *J* = 7.5 Hz, 1 H), 7.57 (m, 1 H), 7.69 (t, *J* = 7.5 Hz, 1 H), 7.77 (dd, *J* = 5.0 Hz, *J* = 1.4 Hz, 1 H), 8.21 (d, *J* = 0.8 Hz, 1 H), 8.60 (d, *J* = 5.0 Hz, 1 H), 9.51 (s, 1 H), 11.54 (s, 1 H) ppm; ^{13}C NMR (DMSO-d_6, 100 Hz) δ: 8.89 (2 C), 14.7, 116.4 (d, *J* = 21.3 Hz), 117.3, 125.2 (d, *J* = 14.5 Hz), 125.6 (d, *J* = 3.0 Hz), 128.9, 132.4 (d, *J* = 1.4 Hz), 132.7 (d, *J* = 8.2 Hz), 135.4, 142.9, 146.2, 148.7, 149.6, 150.1, 157.1, 158.9 (d, *J* = 247.0 Hz), 173.8 ppm; ^{19}F NMR (DMSO-d_6, 376 MHz) δ: -115.9 ppm; ESI-MS *m/z* calcd. for $C_{19}H_{15}O_3N_5F^+$ $[M+H]^+$ 380.11534, found 380.11577, *m/z* calcd. for $C_{19}H_{14}O_3N_5FNa^+$ $[M+Na]^+$ 402.09729, found 402.09768.

*4.1.2.11. 6-(2-Fluorophenyl)-5-(2-fluoropyridine-4-yl)pyrazine-2-amine **M4**:*

Amine **5b** (50 mg, 0.222 mmol, 1.0 eq.) and 2-fluoropyridine-2-boronic acid (37 mg, 0.266 mmol, 1.2 eq.) were added to a mixture of 2 mL 1,4-dioxane and 350 µl of a 2 M Cs_2CO_3 solution (0.700 mmol, 3.1 eq.). Under argon atmosphere, 16.0 mg (0.022 mmol, 0.1 eq.) Pd(dppf)Cl_2 was added and the reaction mixture was heated 3.5 h at 90 °C and further 4 h at 110 °C. After cooling to room temperature, the reaction mixture was quenched with 70 mL water and extracted with ethyl acetate (4 × 25 mL). The combined organic layers were dried over sodium sulfate, filtered and the solvent was evaporated under reduced pressure. The crude product was purified by column chromatography (SiO_2, ethyl acetate/*n*-hexane, 1/2, v/v) to get **M4** with a yield of 54% (34 mg, 0.120 mmol).

R_f (SiO_2, ethyl acetate/*n*-hexane, 1/1, v/v): 0.35; Mp: 210.5-212.7 °C; ^{1}H NMR ($CDCl_3$, 400 MHz) δ: 5.12 (s, 2 H), 6.95 (s, 1 H), 7.02 (ddd, *J* = 9.6 Hz, *J* = 8.3 Hz, *J* = 1.1 Hz, 1 H), 7.10 (dt, *J* = 5.4 Hz, *J* = 1.7 Hz, 1 H), 7.26 (d, *J* = 6.9 Hz, 1 H), 7.43 (tdd, *J* = 7.2 Hz, *J* = 5.1 Hz, *J* = 1.8 Hz, 1 H), 7.50 (dt, *J* = 7.4 Hz, *J* = 1.8 Hz, 1 H), 8.05 (d, *J* = 5.3 Hz, 1 H), 8.10 (s, 1 H) ppm;

^{13}C NMR ($CDCl_3$, 100 Hz) δ: 108.5 (d, *J* = 38.7 Hz), 116.2 (d, *J* = 21.7 Hz), 120.6 (d, *J* = 3.9 Hz), 124.8 (d, *J* = 3.6 Hz), 126.1 (d, *J* = 14.8 Hz), 131.18, 131.2 (d, *J* = 4.4 Hz), 131.4 (d, *J* = 8.2 Hz), 139.2 (d, *J* = 3.7 Hz), 145.8, 147.1 (d, *J* = 15.2 Hz), 152.0 (d, *J* = 8.3 Hz), 153.4, 159.2 (d, *J* = 249.4 Hz), 163.9 (d, *J* = 237.6 Hz) ppm; ^{19}F NMR ($CDCl_3$, 376 MHz) δ: -114.7, -68.4 ppm; ESI-MS *m/z* calcd. for $C_{15}H_{11}N_4F_2^+$ $[M+H]^+$ 285.0946, found 285.0945, *m/z* calcd. for $C_{15}H_{10}N_4F_2Na^+$ $[M+Na]^+$ 307.0762, found 307.0766.
The logD value of **M4** was calculated with ACD/ChemSketch, Vers. 12.5.

4.2 Radiochemistry

4.2.1. General

No-carrier-added [^{18}F]fluoride was produced via the [$^{18}O(p,n)^{18}F$] nuclear reaction by irradiation of an [^{18}O]H_2O target (Hyox 18 enriched water, Rotem Industries Ltd, Israel) on a Cyclone 18/9 (iba RadioPharma Solutions, Belgium) with fixed energy proton beam using Nirta [^{18}F]fluoride XL target.
Radio thin layer chromatography (radio-TLC) was performed on silica gel (Polygram® SIL G/UV_{254}) pre-coated plates with a mixture of EtOAc/cyclohexane 2/1 (v/v) as eluent. The plates were exposed to storage phosphor screens (BAS-TR2025, FUJIFILM Co., Tokyo, Japan) and recorded using the Amersham Typhoon RGB Biomolecular Imager (GE Healthcare Life Sciences). Images were quantified with the ImageQuant TL8.1 software (GE Healthcare Life Sciences).
Analytical chromatographic separations were performed on a JASCO LC-2000 system, incorporating a PU-2080*Plus* pump, AS-2055*Plus* auto injector (100 µL sample loop), and a UV-2070*Plus* detector coupled with a radioactivity HPLC flow monitor (Gabi Star, raytest Isotopenmessgeräte GmbH). Data analysis was performed with the Galaxie chromatography software (Agilent Technologies) using the chromatograms obtained at 254 nm. A Reprosil-Pur C18-AQ column (250 x 4.6 mm; 5 µm; Dr. Maisch HPLC GmbH; Germany) with ACN/20 mM NH_4OAc aq. (pH 6.8) as eluent mixture and a flow of 1.0 mL/min was used (gradient: eluent A 10% ACN/20 mM NH_4OAc aq.; eluent B 90% ACN/20 mM NH_4OAc aq.; 0–5 min 100% A, 5–30 min up to 100% B, 30–35 min 100% B , 35–37 min up to 100% A, 37–40 min 100% A).
Semi-preparative HPLC separations in the manual syntheses were performed on a JASCO LC-2000 system, incorporating a PU-2080-20 pump, an UV/VIS-2075 detector coupled with a radioactivity HPLC flow monitor whose measurement geometry was slightly modified (Gabi Star, raytest Isotopenmessgeräte GmbH) and a fraction collector (Advantec CHF-122SC). Data analysis was performed with the Galaxie chromatography software (Agilent Technologies) using the chromatograms obtained at 254 nm.
The ammonium acetate and the SDS concentrations stated as 20 mM NH_4OAc aq. and 100 mM aq., respectively, correspond to the concentration in the aqueous component of an eluent mixture.

4.2.2. Radiosyntheses

4.2.2.1. Manual syntheses

No carrier added [^{18}F]fluoride in 1.5 mL water was trapped on a Chromafix® 30 PS-HCO_3^- cartridge (MACHEREY-NAGEL GmbH & Co. KG, Düren, Germany). The activity was eluted with 300 µL of an aqueous solution of potassium carbonate (K_2CO_3, 1.8 mg, 13 µmol) into a 4 mL V-vial and Kryptofix 2.2.2 ($K_{2.2.2}$, 11 mg, 29 µmol) in 1 mL ACN was added. The aqueous [^{18}F]fluoride was azeotropically dried under vacuum and nitrogen flow within 7-10 min using a single mode microwave (75 W, at 50–60 °C, power cycling mode). Two aliquots of ACN (2 x 1.0 mL) were added during the drying procedure and the final complex was dissolved in 500 µL DMSO or DMF ready for labeling. Thereafter, a solution of 1–1.2 mg of precursor in 500 µL DMSO or DMF was added, and the ^{18}F-labeling was performed at different temperatures (120 and 155 °C). To analyze the reaction mixture and to determine radiochemical yields, samples were taken for radio-HPLC and radio-TLC at different time points (5, 10, 15, and 20 min).

After cooling to < 30 °C, the reaction mixture was diluted with 2.5 mL water and 0.5 mL ACN and directly applied to an isocratic semi-preparative RP-HPLC for isolation of **[^{18}F]7a** (40% ACN/20 mM $NH_4OAc_{aq.}$, 8 mL/min, Reprosil-Pur 120 CN, 250 x 20 mm; 10 µm; Dr. Maisch HPLC GmbH; Germany). The collected radiotracer fraction was diluted with 35 mL water to perform final purification by sorption on a Sep-Pak® C18 light cartridge (Waters, Milford, MA, USA) and successive elution with 0.75 mL of ethanol.

4.2.2.2. Automated syntheses

Remote controlled radiosynthesis of **[^{18}F]7a** was performed using a TRACERlab FX2 N synthesizer (GE Healthcare, USA) equipped with a Laboport vacuum pump N810.3FT.18 (KNF Neuburger GmbH, Freiburg, Germany), a BlueShadow UV detector 10D (KNAUER GmbH, Berlin, Germany) and the TRACERlab FX Software.

[^{18}F]Fluoride (3-4 GBq) was trapped on a Chromafix® 30 PS-HCO_3^- cartridge (Figure 7, entry **1**, MACHEREY-NAGEL GmbH & Co. KG, Düren, Germany) and eluted into the reactor with 400 µL of an aqueous solution of potassium carbonate (K_2CO_3, 1.8 mg, 13 µmol, entry **2**). After addition of Kryptofix 2.2.2. in 1 mL ACN (11 mg, 29 µmol, entry **3**), the mixture was azeotropically dried for approximately 10 min. Thereafter, 1.0–1.2 mg of the nitro precursor (**13**) dissolved in 1 mL DMSO (entry **4**) was added, and the reaction mixture was stirred at 150 ^{o}C for 15 min. After cooling, the reaction mixture was diluted with 2.5 mL H_2O and 0.5 mL ACN (entry **5**) and transferred into the injection vial (entry **6**). Semi-preparative HPLC was performed using a Reprosil-Pur 120 CN column (250 x 20 mm; 10 µm; Dr. Maisch HPLC GmbH; Germany) with a solvent composition of 40% ACN/20 mM $NH_4OAc_{aq.}$ at a flow rate of 8.0 mL/min (entry **7**). **[^{18}F]7a** was collected in the dilution vessel (entry **8)** previously loaded with 35 mL H_2O. Final purification was performed by passing the solution through a Sep-Pak® C18 light cartridge (entry **9**), followed by washing with 2 mL water (entry **10**) and elution of **[^{18}F]7a** with 1.2 mL EtOH (entry **11**) into the product vial (entry **12**). The ethanolic solution was transferred out of the hot cell and the solvent was reduced under a gentle argon stream

at 70 °C to a final volume of 10-50 µL. Afterwards the radiotracer was diluted in isotonic saline to obtain a final product containing 10% of EtOH (v/v).

The molar activity was determined on the base of a calibration curve carried out under isocratic HPLC conditions (26% ACN/20 mM NH_4OAc_{aq}; Reprosil-Pur 120 CN 250 x 4.6 mm) using chromatograms obtained at 232 nM as an appropriate maximum of UV absorbance.

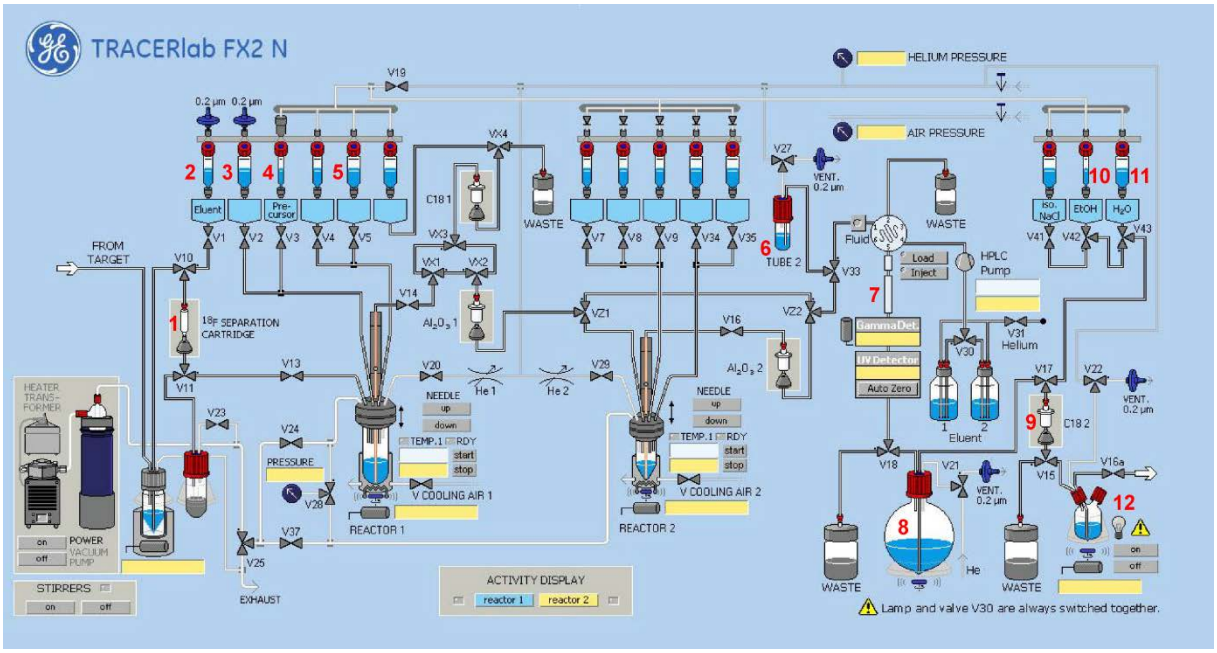

Figure 7. Scheme of the synthesis module TRACERlab FX2 N for the radiosynthesis of **[^{18}F]7a**. (1) Chromafix 30-PS-HCO_3^-, (2) K_2CO_3 (1.8 mg in 400 µL water), (3) $K_{2.2.2.}$ (11 mg in 1 mL ACN), (4) precursor (1 mg of **13** in 1 mL DMSO), (5) 2.5 mL water and 0.5 mL ACN, (6) injection vial, (7) Reprosil-Pur 120 CN (40% ACN/20 mM $NH_4OAc_{aq.}$, flow 8.0 mL/min), (8) 35 mL water, (9) Sep-Pak® C18 light, (10) 2 mL water, (11) 1.2 mL EtOH, (12) product vial.

4.2.2.3. In vitro stability and determination of logD value

The in vitro stability of **[^{18}F]7a** was investigated by incubation of small tracer amounts (~ 5 MBq) at 40 °C in i) 500 µL *n*-octanol and ii) 500 µL pig plasma samples. After 30 and 60 min, aliquots were taken and analyzed by radio-TLC and radio-HPLC. The plasma samples were processed as described in 4.4.3.

The partition coefficient of **[^{18}F]7a** was experimentally determined for the *n*-octanol/PBS system by the shake-flask method. Small tracer amounts (~ 800 kBq) were added to a mixture of 3.0 mL of *n*-octanol and 3.0 mL of PBS. After shaking for 20 min at room temperature, the samples were centrifuged (10,000 rpm, 5 min) and 1 mL aliquots of the organic as well as the aqueous layer were taken and measured in a gamma counter (PerkinElmer Wallac Wizard 1480 Gamma Counter, manufactured by WALLAC, Turku, Finland). Another 1 mL aliquote of the organic layer was mixed with 2.0 mL *n*-octanol and 3.0 mL of PBS and subjected to the same procedure until constant partition coefficient values had been obtained. All measurements were done in quadruplicate.

4.3. In vitro binding assays

4.3.1. Determination of K_i values

Membrane preparations of recombinant CHO or HEK (human embryonic kidney) cells expressing the respective human adenosine receptor subtype were obtained according to Borrman *et al.* [28] or purchased from Perkin Elmer. Radioligand binding assays at human A_1, A_{2A}, A_{2B} and A_3 receptors were performed according to Alnouri *et al*.[48]

The following radioligands were employed: [^{3}H]2-chloro-N^{6}cyclopentyladenosine ([^{3}H]CCPA, 1 nM[49]) for the A_1 receptor, [^{3}H]3-(3-hydroxypropyl)-7-methyl-8-(*m*-methoxystyryl)-1-propargylxanthine ([^{3}H]MSX-2, 1 nM[50]) for the A_{2A} receptor, [^{3}H]8-(4-[4-(4-chlorophenyl)piperazine-1-sulfonyl]phenyl)-1-propyl-2,3,6,7-tetrahydro-1*H*-purine-2,6-dione ([^{3}H]PSB-603, 0.3 nM[28]) for the A_{2B} receptor, and [^{3}H](*R*)-8-ethyl-4-methyl-2-(phenyl)1,4,7,8-tetrahydro-5*H*-imidazo[2,1-*i*]purin-5-one ([^{3}H]PSB-11, 1 nM[51]) for the A_3 receptor. Three separate experiments were performed for determination of K_i values. All data were analyzed with GraphPad Prism, Version 4.1 (GraphPad Inc., La Jolla, CA).

4.3.2. Binding of [^{18}F]7a to mouse tissue

Mouse tissue samples were prepared by homogenizing the brain and heart from female CD-1 mice (10-12 weeks) with homogenization buffer (50 mM TRIS-HCl, pH 7.4) on ice using a Potter S homogenizer (B. Braun Biotech, Göttingen, Germany). 10 mL buffer were added to 1 g tissue in a borosilicate vessel with a PTFE plunger and the biological material disrupted by up and down movement of the pestle (10 repetitions), rotating at 1500 rpm. The suspension was centrifuged at 12000 rpm for 10 min at 4 °C (3-30KS, Sigma Laborzentrifugen GmbH, Osterode am Harz, Germany). The pellet was re-suspended in homogenization buffer and centrifuged as described. After repeating this washing step, the sediment was suspended in the initial volume of homogenization buffer and stored in aliquots of 1 mL at -25 °C. For the experiment, the tissue homogenates were thawed and incubated at 560 µg protein/mL (Pierce BCA Protein Assay; Thermo Fisher Scientific, Dreieich, Germany) with 0.275 MBq/mL of **[^{18}F]7a** (4 nM at start of incubation) in incubation buffer (50 mM TRIS-HCl, pH 7.4, 100 mM NaCl, 5 mM $MgCl_2$, 1 mM EDTA) with continuous shaking at room temperature. The binding experiments were performed in the presence of recombinant human adenosine deaminase at a working concentration of 1 U/L. To assess non-specific binding of **[^{18}F]7a**, co-incubations with either 1 µM **7a** or 1 µM PSB-603 were performed. To assess filter-binding of **[^{18}F]7a**, incubations without tissue homogenates were performed. The incubation was terminated after 60 min by filtration via a glass microfibre filter (Whatman grade GF-B; GE Healthcare via Fisher Scientific GmbH, Schwerte, Germany), pre-incubated for 60 min with freshly prepared 0.3% polyethyleneimine, using a 48-well cell harvester (Brandel Harvesters, Brandel, Gaithersburg, MD, USA). Activity trapped on the filters was counted using a gamma counter (2480 Wizard2™, PerkinElmer LAS GmbH, Germany).

4.4. In vivo / ex vivo studies

Animals for in vivo studies were obtained from the Medizinisch-Experimentelles Zentrum, Universität Leipzig. All procedures that include animals were approved by the respective State Animal Care and Use committee and conducted in accordance with the German Law for the Protection of Animals (TVV 08/13).

4.4.1. Ex vivo autoradiography of [^{18}F]7a in mice

[^{18}F]7a was administered as bolus in one awake female CD-1 mouse (12 weeks, 32.5 g) via the tail vein (4 MBq and 31 nmol/kg at time of injection). The brain was isolated after cervical dislocation of the anesthetized animal at 30 min p.i., and the two hemispheres separated and frozen immediately in pre-cooled isopentane at -25°C for 10 min. Cryosections of 12 µm were obtained using a cryostat microtome (Microm HM 560 Cryostat, Microm International GmbH, Walldorf, Germany) and mounted on microscope slides. After drying for 10 min under a stream of cold air, the sections were exposed to an imaging plate (FUJIFILM Corporation, Tokyo, Japan) for 120 min. Afterwards, the imaging plate was read out (HD-CR 35 NDT, DÜRR NDT GmbH & Co. KG, Bietigheim-Bissingen, Germany) and the digital image analysed using AIDA Image Analysis software (V 4.27; Elysia-raytest GmbH, Straubenhardt, Germany). Eventually the brain sections were Nissl-stained and scanned (Super COOLSCAN 9000 ED, Nikon GmbH, Düsseldorf, Germany) to delineate brain regions using a mouse brain atlas.[52]

4.4.2. Dynamic PET scan of [^{18}F]7a in mice

One female CD-1 mouse (12 weeks, 33 g) was initially anesthetized with 4 % of isoflurane and was positioned prone in a small-animal PET/MRI system (nanoScan®, MEDISO, Budapest, Hungary) equipped with respiratory monitoring, heated mouse bed (37 °C), and inhalation anesthesia (1.8 % isoflurane in a 60 % oxygen/40 % air gas mixture at 250 ml/min airflow; Anesthesia Unit U-410, agntho's, Lidingö, Sweden; Gas blender 100 series, MCQ Instruments, Rome, Italy). Prior to the PET scan a scout image MR sequence was done to outline the animal dimensions. The animal was injected via the tail vein with 3.2 MBq **[^{18}F]7a** (15 nmol/kg at time of injection) in a volume of 200 µl saline. The injected dose was calculated by the difference of the activity in the syringe before and after the injection. A dynamic whole body animal PET scan of 60 min length was started simultaneously. The list-mode data was sorted into sinograms using a framing scheme of 6 × 10 s, 6 × 30 s, 5 × 60 s, 10 × 300 s frames and reconstructed by OSEM3D with 4 iterations and 6 subsets. A mouse brain atlas (PMOD (v.3.7, PMOD technologies LLC, Zurich, Switzerland) was used to delineate regions of interest.

4.4.3. Metabolism studies of [^{18}F]7a in mice

[^{18}F]7a was administered as bolus in awake female CD-1 mice (10-12 weeks, 25-32 g) via the tail vein (10-80 MBq and 1-50 nmol/kg at time of injection). At 5 (n=2), 15 (n=2), and 30 (n=3) min p.i., blood samples were obtained retro-orbitally from the anesthetized animals. Blood plasma was obtained as supernatant after centrifugation of the whole blood samples

(14000 rpm, 1 min; Centrifuge 5418, Eppendorf Vertrieb Deutschland GmbH, Wesseling-Berzdorf, Germany). After cervical dislocation, the brains were isolated immediately, and urine samples obtained. All samples were weighed and the respective activity measured in a dose calibrator (ISOMED 2010; MED Nuklear-Medizintechnik Dresden GmbH, Dresden, Germany). Afterwards, 1 mL of deionized water was added to the brain in a borosilicate vessel with a PTFE plunger and the biological material was homogenized on ice by repeated up and down movement of the pestle, rotating at 1500 rpm.

MLC: For preparation of the MLC injection samples, mouse plasma (20 – 50 µL) was dissolved in 100 – 300 µL of 200 mM aqueous SDS. Homogenized brain material (100 – 200 µL) was dissolved in 500 µL of 200 mM aqueous SDS, stirred at 75 °C for 5 minutes, diluted with further 200 µL of 200 mM aqueous SDS and injected into the MLC system after cooling to room temperature. The MLC system was built up of a JASCO PU-980 pump, an AS-2055*Plus* auto injector with a 2000 µL sample loop, and a UV-1575 detector coupled with a gamma radioactivity HPLC detector (Gabi Star, raytest Isotopenmessgeräte GmbH). Data analysis was performed with the Galaxie chromatography software (Agilent Technologies). A Reprosil-Pur C18-AQ column (250 x 4.6 mm, particle size: 10 µm) coupled with a pre-column of 10 mm length was used. Separations were performed by using an eluent mixture of THF/100 mM aqueous SDS/10mM Na_2HPO_4 aq. in gradient mode (0 – 10 min at 100% 100 mM aqueous SDS, 10 – 25 min up to 50% THF, 25 – 30 min at 50% THF, 30 – 31 min up to 100% 100 mM aqueous SDS; 31 – 40 min at 100% 100 mM aqueous SDS) at a flow rate of 1.0 mL/min.

RP-HPLC: Protein precipitation was performed by addition of an ice-cold mixture of acetone/water (9/1; v/v) in a ratio of 4 : 1 (v/v) of organic solvent to plasma or brain homogenate, respectively. The samples were vortexed for 3 min, equilibrated on ice for 5 min, and centrifuged for 5 min at 10,000 rpm. The precipitates were washed with 100 µL of the solvent mixture and subjected to the same procedure. The combined supernatants (total volume between 1.0 –1.5 mL) were concentrated at 65 °C under argon flow to a final volume of approximately 100 µL and analyzed by analytical radio-HPLC. To determine the percentage of activity in the supernatants compared to total activity, aliquots of each step as well as the precipitates were quantified by γ counting (PerkinElmer Wallac Wizard 1480 Gamma Counter, manufactured by WALLAC, Turku, Finland). For plasma samples recoveries of 97% of total activity for the 5 min samples and 87-85% for the 15 and 30 min samples were obtained indicating the formation of [^{18}F]fluoride which could not be entirely extracted from the protein precipitates. Independent from the sampling time, 96-97% of recoveries were obtained for the brain samples. To analyze the samples, the same HPLC method was used as described in the radiochemistry part.

4.5. Molecular modelling studies

4.5.1. Homology model of the A_{2B} receptor

A homology model of the human adenosine A_{2B} receptor based on the X-ray crystal structure of the human adenosine A_{2A} receptor was recently described.[34] The A_{2A} receptor structure was used as a template for generating a homology model of the A_{2B} receptor using

Modeller9.[53, 54] The selected A_{2A} receptor template co-crystallized with the antagonist ZM241385 (PDB ID: 4EIY, resolution: 1.8 Å) was downloaded from the Protein Data Bank.[55] The amino acid sequence of the A_{2B} receptor with the accession number of P29275 was retrieved from the UniProt sequence database (http://www.uniprot.org/). The sequence similarity of 73.1% and sequence identity of 58.3% between the A_{2B} and the A_{2A} receptors and high resolution of the A_{2A} receptor crystal structure justified the choice of this structure as a template for the homology model. For each model, the variable target function method with conjugate gradients in Modeller was applied to optimize the model, followed by refinement using molecular dynamics with a simulated annealing method. Discrete Optimized Protein Energy (DOPE) score was utilized to select the best model of A_{2B} from the 100 generated models.[54] The protonation of the selected model was achieved using the Protonate3D algorithm applying Molecular Operating Environment (MOE 2016.08) followed by minimization with a root mean square of 0.5 Å.[56]

4.5.2. Molecular docking

The selected homology model of the A_{2B} receptor was applied for flexible ligand docking using the molecular docking program, AutoDock 4.2.[57] During the docking simulations, the ligands were fully flexible while the residues of the receptor were treated as rigid. In order to predict the binding modes of the compounds, selected compounds were docked into the active site of the A_{2B} receptor. The atomic partial charges were added using AutoDockTools.[57, 58] Fifty independent docking calculations using the *var*CPSO-ls algorithm from PSO@Autodock implemented in AutoDock4.2 were performed and terminated after 500,000 evaluation steps.[59] Parameters of *var*CPSO-ls algorithm, the cognitive and social coefficients c1 and c2 were set at 6.05 with 60 individual particles as swarm size. All the other parameters of the algorithm were set at their default values. Possible binding modes of the compounds were explored by visual inspection of the resulting docking poses.

Acknowledgements

The authors would like to thank the BMBF (German Federal Ministry for Education and Research) for the financial support within the BioPharma initiative “Neuroallianz” (D11B project).

We also thank Dr. K. Franke, Dr. A. Mansel and Dr. S. Fischer for providing [^{18}F]fluoride and T. Spalholz for her help with the in vitro studies. We are thankful to Dr. L. Hennig, Dr. S. Billig and R. Oehme from the University of Leipzig for measuring the NMR and high resolution mass spectra. We thank A. Fischer and A. Püsche for performing radioligand binding assays. We are very thankful to Dr. D. Thimm for his support in the project management.

Supplementary data

Supplementary data related to this article can be found in the online version.

These data include NMR and MS spectra, LC-MS chromatograms and the sequence alignment of human adenosine receptor subtypes.

References

1. Antonioli, L.; Pacher, P.; Vizi, E. S.; Hasko, G. CD39 and CD73 in immunity and inflammation. *Trends Mol. Med.* **2013,** *19*, 355.
2. Fredholm, B. B.; IJzerman, A. P.; Jacobson, K. A.; Linden, J.; Müller, C. E. International Union of Basic and Clinical Pharmacology. LXXXI. Nomenclature and Classification of Adenosine Receptors-An Update. *Pharmacol. Rev.* **2011,** *63*, 1.
3. Fredholm, B. B.; IJzerman, A. P.; Jacobson, K. A.; Klotz, K. N.; Linden, J. International Union of Pharmacology. XXV. Nomenclature and classification of adenosine receptors. *Pharmacol. Rev.* **2001,** *53*, 527.
4. Müller, C. E.; Baqi, Y.; Hinz, S.; Namasivayam, V. In *The adenosine receptors;* Borea, P. A., Varani, K., Eds.; Springer Science, in press, 2018.
5. Fredholm, B. B.; Irenius, E.; Kull, B.; Schulte, G. Comparison of the potency of adenosine as an agonist at human adenosine receptors expressed in Chinese hamster ovary cells. *Biochem. Pharmacol.* **2001,** *61*, 443.
6. Feoktistov, I.; Biaggioni, I. Adenosine A_{2B} receptors. *Pharmacol. Rev.* **1997,** *49*, 381.
7. Antonioli, L.; Blandizzi, C.; Pacher, P.; Hasko, G. Immunity, inflammation and cancer: a leading role for adenosine. *Nat. Rev. Cancer* **2013,** *13*, 842.
8. Sepulveda, C.; Palomo, I.; Fuentes, E. Role of adenosine A_{2B} receptor overexpression in tumor progression. *Life Sci.* **2016,** *166*, 92.
9. Sorrentino, C.; Morello, S. Role of adenosine in tumor progression: focus on A_{2B} receptor as potential therapeutic target. *J. Cancer Metastasis Treat.* **2017,** *3*, 127.
10. Ryzhov, S.; Novitskiy, S. V.; Zaynagetdinov, R.; Goldstein, A. E.; Carbone, D. P.; Biaggioni, I.; Dikov, M. M.; Feoktistov, I. Host A_{2B} adenosine receptors promote carcinoma growth. *Neoplasia* **2008,** *10*, 987.
11. Cacciari, B.; Pastorin, G.; Bolcato, C.; Spalluto, G.; Bacilieri, M.; Moro, S. A_{2B} adenosine receptor antagonists: Recent developments. *Mini-Rev. Med. Chem.* **2005,** *5*, 1053.
12. Sachdeva, S.; Gupta, M. Adenosine and its receptors as therapeutic targets: An overview. *Saudi Pharm. J.* **2013,** *21*, 245.
13. Dixon, A. K.; Gubitz, A. K.; Sirinathsinghji, D. J.; Richardson, P. J.; Freeman, T. C. Tissue distribution of adenosine receptor mRNAs in the rat. *Br. J. Pharmacol.* **1996,** *118*, 1461.
14. Stehle, J. H.; Rivkees, S. A.; Lee, J. J.; Weaver, D. R.; Deeds, J. D.; Reppert, S. M. Molecular cloning and expression of the cDNA for a novel A_2-adenosine receptor subtype. *Mol. Endocrinol.* **1992,** *6*, 384.
15. Panjehpour, M.; Castro, M.; Klotz, K. N. Human breast cancer cell line MDA-MB-231 expresses endogenous A_{2B} adenosine receptors mediating a Ca^{2+} signal. *Br. J. Pharmacol.* **2005,** *145*, 211.
16. Ma, D. F.; Kondo, T.; Nakazawa, T.; Niu, D. F.; Mochizuki, K.; Kawasaki, T.; Yamane, T.; Katoh, R. Hypoxia-inducible adenosine A_{2B} receptor modulates proliferation of colon carcinoma cells. *Hum. Pathol.* **2010,** *41*, 1550.
17. Kalhan, A.; Gharibi, B.; Vazquez, M.; Jasani, B.; Neal, J.; Kidd, M.; Modlin, I. M.; Pfragner, R.; Rees, D. A.; Ham, J. Adenosine A_{2A} and A_{2B} receptor expression in neuroendocrine tumours: potential targets for therapy. *Purinergic Signal.* **2012,** *8*, 265.

18. Mousavi, S.; Panjehpour, M.; Izadpanahi, M. H.; Aghaei, M. Expression of adenosine receptor subclasses in malignant and adjacent normal human prostate tissues. *Prostate* **2015,** *75*, 735.
19. Zeng, D. W.; Maa, T.; Wang, U.; Feoktistov, I.; Biaggioni, I.; Belardinelli, L. Expression and function of A_{2B} adenosine receptors in the U87MG tumor cells. *Drug Dev. Res.* **2003,** *58*, 405.
20. Gessi, S.; Varani, K.; Merighi, S.; Cattabriga, E.; Pancaldi, C.; Szabadkai, Y.; Rizzuto, R.; Klotz, K. N.; Leung, E.; Mac Lennan, S.; Baraldi, P. G.; Borea, P. A. Expression, pharmacological profile, and functional coupling of A_{2B} receptors in a recombinant system and in peripheral blood cells using a novel selective antagonist radioligand, [^{3}H]MRE 2029-F20. *Mol. Pharmacol.* **2005,** *67*, 2137.
21. Hinz, S.; Navarro, G.; Borroto-Escuela, D.; Seibt, B. F.; Ammon, Y. C.; de Filippo, E.; Danish, A.; Lacher, S. K.; Cervinkova, B.; Rafehi, M.; Fuxe, K.; Schiedel, A. C.; Franco, R.; Müller, C. E. Adenosine A_{2A} receptor ligand recognition and signaling is blocked by A_{2B} receptors. *Oncotarget* **2018,** *9*, 13593.
22. Kalla, R. V.; Zablocki, J.; Tabrizi, M. A.; Baraldi, P. G. Recent developments in A_{2B} adenosine receptor ligands. *Handb. Exp. Pharmacol.* **2009**, 99.
23. Müller, C. E.; Jacobson, K. A. Recent developments in adenosine receptor ligands and their potential as novel drugs. *Biochim. Biophys. Acta* **2011,** *1808*, 1290.
24. Ortore, G.; Martinelli, A. A_{2B} receptor ligands: past, present and future trends. *Curr. Top. Med. Chem.* **2010,** *10*, 923.
25. Kim, Y. C.; Ji, X.; Melman, N.; Linden, J.; Jacobson, K. A. Anilide derivatives of an 8-phenylxanthine carboxylic congener are highly potent and selective antagonists at human A_{2B} adenosine receptors. *J. Med. Chem.* **2000,** *43*, 1165.
26. Hayallah, A. M.; Sandoval-Ramirez, J.; Reith, U.; Schobert, U.; Preiss, B.; Schumacher, B.; Daly, J. W.; Müller, C. E. 1,8-disubstituted xanthine derivatives: synthesis of potent A_{2B}-selective adenosine receptor antagonists. *J. Med. Chem.* **2002,** *45*, 1500.
27. Elzein, E.; Kalla, R. V.; Li, X.; Perry, T.; Gimbel, A.; Zeng, D.; Lustig, D.; Leung, K.; Zablocki, J. Discovery of a novel A_{2B} adenosine receptor antagonist as a clinical candidate for chronic inflammatory airway diseases. *J. Med. Chem.* **2008,** *51*, 2267.
28. Borrmann, T.; Hinz, S.; Bertarelli, D. C.; Li, W.; Florin, N. C.; Scheiff, A. B.; Müller, C. E. 1-Alkyl-8-(piperazine-1-sulfonyl)phenylxanthines: Development and characterization of adenosine A_{2B} receptor antagonists and a new radioligand with subnanomolar affinity and subtype specificity. *J. Med. Chem.* **2009,** *52*, 3994.
29. Eastwood, P.; Esteve, C.; Gonzalez, J.; Fonquerna, S.; Aiguade, J.; Carranco, I.; Domenech, T.; Aparici, M.; Miralpeix, M.; Alberti, J.; Cordoba, M.; Fernandez, R.; Pont, M.; Godessart, N.; Prats, N.; Loza, M. I.; Cadavid, M. I.; Nueda, A.; Vidal, B. Discovery of LAS101057: A Potent, Selective, and Orally Efficacious A_{2B} Adenosine Receptor Antagonist. *ACS Med. Chem. Lett.* **2011,** *2*, 213.
30. Vidal, B.; Nueda, A.; Esteve, C.; Domenech, T.; Benito, S.; Reinoso, R. F.; Pont, M.; Calbet, M.; Lopez, R.; Cadavid, M. I.; Loza, M. I.; Cardenas, A.; Godessart, N.; Beleta, J.; Warrellow, G.; Ryder, H. Discovery and characterization of 4'-(2-furyl)-N-pyridin-3-yl-4,5'-bipyrimidin-2'-amine (LAS38096), a potent, selective, and efficacious A_{2B} adenosine receptor antagonist. *J. Med. Chem.* **2007,** *50*, 2732.
31. El Maatougui, A.; Azuaje, J.; Gonzalez-Gomez, M.; Miguez, G.; Crespo, A.; Carbajales, C.; Escalante, L.; Garcia-Mera, X.; Gutierrez-de-Teran, H.; Sotelo, E. Discovery of Potent and Highly Selective A_{2B} Adenosine Receptor Antagonist Chemotypes. *J. Med. Chem.* **2016,** *59*, 1967.

32. Petroni, D.; Giacomelli, C.; Taliani, S.; Barresi, E.; Robello, M.; Daniele, S.; Bartoli, A.; Burchielli, S.; Pardini, S.; Salvadori, P. A.; Da Settimo, F.; Martini, C.; Trincavelli, M. L.; Menichetti, L. Toward PET imaging of A_{2B} adenosine receptors: a carbon-11 labeled triazinobenzimidazole tracer: Synthesis and imaging of a new A_{2B} PET tracer. *Nucl. Med. Biol.* **2016,** *43*, 309.
33. Vidal, B.; Esteve, C.; Soca, L.; Eastwood, P. R., in: WO 2007/017096; **2007**, 198.
34. Köse, M.; Gollos, S.; Karcz, T.; Fiene, A.; Heisig, F.; Behrenswerth, A.; Kiec-Kononowicz, K.; Namasivayam, V.; Müller, C. E. Fluorescent-Labeled Selective Adenosine A_{2B} Receptor Antagonist Enables Competition Binding Assay by Flow Cytometry. *J. Med. Chem.* **2018,** *61*, 4301.
35. Wagner, S.; Teodoro, R.; Deuther-Conrad, W.; Kranz, M.; Scheunemann, M.; Fischer, S.; Wenzel, B.; Egerland, U.; Hoefgen, N.; Steinbach, J.; Brust, P. Radiosynthesis and biological evaluation of the new PDE10A radioligand [^{18}F]AQ28A. *J. Labelled Compd. Radiopharm.* **2017,** *60*, 36.
36. Yanguo, L.; Xuemin, F.; Donzhao, W. in: CN 108047258 Patent; **2018**.
37. Wiley, R. H.; Hartman, J. L. Oxidation of Aminopyridines to Nitropyridines. *J. Am. Chem. Soc.* **1951,** *73*, 494.
38. Teodoro, R.; Wenzel, B.; Oh-Nishi, A.; Fischer, S.; Peters, D.; Suhara, T.; Deuther-Conrad, W.; Brust, P. A high-yield automated radiosynthesis of the alpha-7 nicotinic receptor radioligand [^{18}F]NS10743. *Appl. Radiat. Isot.* **2015,** *95*, 76.
39. A Reprosil-Gold (strong hydrophobic phase) and a Reprosil-Pur C18 AQ (hydrophobic, polar phase) column from the Dr. Maisch company have been used.
40. Rankovic, Z. CNS drug design: balancing physicochemical properties for optimal brain exposure. *J. Med. Chem.* **2015,** *58*, 2584.
41. Pike, V. W. Considerations in the development of reversibly binding PET radioligands for brain imaging. *Curr. Med. Chem.* **2016,** *23*, 1818.
42. Brust, P.; van den Hoff, J.; Steinbach, J. Development of ^{18}F-labeled radiotracers for neuroreceptor imaging with positron emission tomography. *Neurosci. Bull.* **2014,** *30*, 777.
43. Chen, J. F.; Moratalla, R.; Impagnatiello, F.; Grandy, D. K.; Cuellar, B.; Rubinstein, M.; Beilstein, M. A.; Hackett, E.; Fink, J. S.; Low, M. J.; Ongini, E.; Schwarzschild, M. A. The role of the D_2 dopamine receptor (D_2R) in A_{2A} adenosine receptor ($A_{2A}R$)-mediated behavioral and cellular responses as revealed by A_{2A} and D_2 receptor knockout mice. *Proc. Natl. Acad. Sci. U S A* **2001,** *98*, 1970.
44. Masino, S.; Boison, D. *Adenosine: A key link between metabolism and brain activity*: Springer, 2013.
45. Cabiati, M.; Martino, A.; Mattii, L.; Caselli, C.; Prescimone, T.; Lionetti, V.; Morales, M. A.; Del Ry, S. Adenosine receptor expression in an experimental animal model of myocardial infarction with preserved left ventricular ejection fraction. *Heart Vessels* **2014,** *29*, 513.
46. Epperson, S. A.; Brunton, L. L.; Ramirez-Sanchez, I.; Villarreal, F. Adenosine receptors and second messenger signaling pathways in rat cardiac fibroblasts. *Am. J. Physiol. Cell. Physiol.* **2009,** *296*, C1171.
47. Khaledi, M. G. Micelles as separation media in high-performance liquid chromatography and high-performance capillary electrophoresis: overview and perspective. *J. Chromat. A* **1997,** *780*, 3.
48. Alnouri, M. W.; Jepards, S.; Casari, A.; Schiedel, A. C.; Hinz, S.; Müller, C. E. Selectivity is species-dependent: Characterization of standard agonists and antagonists at human, rat, and mouse adenosine receptors. *Purinergic Signal.* **2015,** *11*, 389.

49. Klotz, K. N.; Lohse, M. J.; Schwabe, U.; Cristalli, G.; Vittori, S.; Grifantini, M. 2-Chloro-N6-[^{3}H]cyclopentyladenosine ([^{3}H]CCPA)-a high affinity agonist radioligand for A_1 adenosine receptors. *Naunyn Schmiedebergs Arch. Pharmacol.* **1989,** *340*, 679.
50. Müller, C. E.; Maurinsh, J.; Sauer, R. Binding of [^{3}H]MSX-2 (3-(3-hydroxypropyl)-7-methyl-8-(m-methoxystyryl)-1-propargylxanthine) to rat striatal membranes-a new, selective antagonist radioligand for A_{2A} adenosine receptors. *Eur. J. Pharm. Sci.* **2000,** *10*, 259.
51. Müller, C. E.; Diekmann, M.; Thorand, M.; Ozola, V. [^{3}H]8-Ethyl-4-methyl-2-phenyl-(8R)-4,5,7,8-tetrahydro-1H-imidazo[2,1-i]-purin-5-one ([^{3}H]PSB-11), a novel high-affinity antagonist radioligand for human A_3 adenosine receptors. *Bioorg. Med. Chem. Lett.* **2002,** *12*, 501.
52. Paxinos, G.; Keith, B. J. F. The mouse brain in stereotaxic coordinates.
53. Sali, A.; Blundell, T. L. Comparative protein modelling by satisfaction of spatial restraints. *J. Mol. Biol.* **1993,** *234*, 779.
54. Shen, M. Y.; Sali, A. Statistical potential for assessment and prediction of protein structures. *Protein Sci.* **2006,** *15*, 2507.
55. Dore, A. S.; Robertson, N.; Errey, J. C.; Ng, I.; Hollenstein, K.; Tehan, B.; Hurrell, E.; Bennett, K.; Congreve, M.; Magnani, F.; Tate, C. G.; Weir, M.; Marshall, F. H. Structure of the adenosine A_{2A} receptor in complex with ZM241385 and the xanthines XAC and caffeine. *Structure* **2011,** *19*, 1283.
56. Molecular Operating Environment (MOE 2016.8). Chemical computing group, Montreal, Quebec, Canada.
57. Morris, G. M.; Huey, R.; Lindstrom, W.; Sanner, M. F.; Belew, R. K.; Goodsell, D. S.; Olson, A. J. AutoDock4 and AutoDockTools4: Automated docking with selective receptor flexibility. *J. Comput. Chem.* **2009,** *30*, 2785.
58. Sanner, M. F. Python: a programming language for software integration and development. *J. Mol. Graph. Model.* **1999,** *17*, 57.
59. Namasivayam, V.; Günther, R. PSO@autodock: A fast flexible molecular docking program based on Swarm intelligence. *Chem. Biol. Drug Des.* **2007,** *70*, 475.